Title

The myeloid type I interferon response to myocardial infarction begins in bone marrow and is regulated by Nrf2-activated macrophages

Journal

Science Immunology, 5(51)

ISSN

2470-9468

Authors

Calcagno, David M
Ng, Richard P
Toomu, Avinash
et al.

Publication Date

2020-09-18

DOI

10.1126/sciimmunol.aaz1974

Peer reviewed

HHS Public Access

Author manuscript

Sci Immunol. Author manuscript; available in PMC 2021 March 25.

Published in final edited form as:

Sci Immunol. 2020 September 25; 5(51): . doi:10.1126/sciimmunol.aaz1974.

The myeloid type I interferon response to myocardial infarction begins in bone marrow and is regulated by Nrf2-activated macrophages

David M. Calcagno[1,*], **Richard P. Ng Jr.**[2,*], **Avinash Toomu**[2], **Claire Zhang**[1], **Kenneth Huang**[2], **Aaron D. Aguirre**[3,4,5], **Ralph Weissleder**[4], **Lori B. Daniels**[2], **Zhenxing Fu**[2], **Kevin R. King**[1,2]

[1]Department of Bioengineering, Jacobs School of Engineering, University of California San Diego, La Jolla, CA, USA.

[2]Division of Cardiology and Cardiovascular Institute, Department of Medicine, University of California San Diego, La Jolla, CA, USA.

[3]Cardiology Division, Massachusetts General Hospital, Harvard Medical School, Boston, Massachusetts, USA.

[4]Center for Systems Biology, Massachusetts General Hospital, Harvard Medical School, Boston, Massachusetts, USA.

[5]Wellman Center for Photomedicine, Massachusetts General Hospital, Harvard Medical School, Boston, Massachusetts, USA.

Abstract

Sterile tissue injury is thought to locally activate innate immune responses via damage associated molecular patterns (DAMPs). Whether innate immune pathways are remotely activated remains relatively unexplored. Here, by analyzing ~145,000 single cell transcriptomes at steady state and after myocardial infarction (MI) in mice and humans, we show that the type I interferon (IFN) response, characterized by expression of interferon-stimulated genes (ISGs), begins far from the site of injury, in neutrophil and monocyte progenitors within the bone marrow. In the peripheral blood of patients, we observed defined subsets of ISG-expressing neutrophils and monocytes. In the bone marrow and blood of mice, ISG expression was detected in neutrophils and monocytes and their progenitors; intensified with maturation at steady-state and after MI; and was controlled by Tet2 and Irf3 transcriptional regulators. Within the infarcted heart, ISG-expressing cells were negatively regulated by Nrf2 activation in Ccr2^{-} steady-state cardiac macrophages. Our results

Corresponding author: Kevin R. King, MD, PhD, University of California San Diego, 9500 Gilman Dr. MC 0412, La Jolla, CA 92093, Tel: 617-869-9339, krking@ucsd.edu.

Author Contributions. All authors designed and performed the experiments and analyzed the data. D.M.C., R.P.N., Jr., and K.R.K. wrote the manuscript. All authors reviewed results and revised the manuscript.

*Authors contributed equally.

Competing Interests. K.R.K. has served as a consultant for MedImmune and AstraZeneca. The other authors declare they have no competing financial interests.

Data and Materials Availability. The single cell RNA sequencing data has been deposited to the NCBI GEO database and is available under accession number GSE157244. All other data needed to evaluate the conclusions in the paper are present in the paper or the Supplementary Materials. Requests for materials should be addressed to K.R.K. (krking@ucsd.edu).

show that IFN signaling begins in the bone marrow, implicate multiple transcriptional regulators (Tet2, Irf3, Nrf2) in governing ISG expression, and provide a clinical biomarker (ISG score) for studying IFN signaling in patients.

Introduction

Ischemic tissue injury is the initiating event underlying the most common causes of death in the world(1). In the heart, acute ischemia causes myocardial infarction (MI), which provokes a distant emergency myelopoietic response in the bone marrow that rapidly increases production of neutrophils and monocytes, and leads to peripheral blood leukocytosis, tissue infiltration, and organ dysfunction (e.g. heart failure), the hallmarks of acute inflammation (2–7).

In response to ischemic injury, myeloid cells infiltrate the heart as overlapping waves of neutrophils and monocytes. Neutrophils, which peak at post-MI days 1–2, generate reactive oxygen species, elaborate protease- and myeloperoxidase-containing granules, and are thought to exacerbate tissue damage (8). Although protective neutrophil subsets have also been proposed, the full functional diversity of infarct neutrophils remains largely unexplored (9, 10). Monocytes, which peak at post-MI days 3–4, infiltrate and differentiate into functionally heterogeneous $Ccr2^{+}$ macrophage subsets with both proinflammatory and reparative phenotypes (2, 8, 11, 12). Also present within the infarct are $Ccr2^{-}$ steady-state macrophages, which are proposed to play protective roles by incompletely understood mechanisms (13–15). Broadly speaking, myeloid cells are thought to develop their specialized effector functions *locally,* as a consequence of interactions with damage associated molecular patterns (DAMPs), cytokines, and other stimuli within the injured tissue microenvironment (16, 17). Here, we examined the possibility that innate immune pathways are activated *remotely*, prior to infiltrating the infarcted heart.

The type I IFN response is an innate immune pathway best known for its roles in the anti-viral response and its association with auto-inflammatory diseases such as lupus (18–20). We and others recently discovered that pathologic type I IFN responses also occur after ischemic injury in the heart (21, 22). We showed that genetic or pharmacologic inhibition of IFN signaling reduced inflammation, limited adverse ventricular remodeling, and improved survival in mice (21, 22). Circumstantial evidence localized the response to monocyte-derived macrophages within the infarcted heart; however, this was not directly confirmable in patients due to inherent dangers associated with biopsying the recently infarcted human heart. Therefore, our data did not completely rule out activation in the blood or bone marrow, prior to arrival at the heart. Here, we hypothesize that peripheral blood myeloid cells exhibit functional heterogeneity prior to entering the heart, and that it went unnoticed in previous studies because of reliance on ensemble measurement techniques (e.g. qPCR and bulk RNA-seq). To test this hypothesis, we performed single cell RNA-seq analysis of the bone marrow, blood, and heart after MI (23) and defined the origins, regulation, and human relevance of type I IFN signaling at steady state and after MI.

Our results show that myeloid IFN responses begin remotely, in the distant bone marrow, at the origins of emergency myelopoiesis. We analyzed ~145,000 single cell transcriptomes

from the hearts, blood, and bone marrow of mice and humans to define the intracardiac states, trajectories, and inducible programs of post-MI neutrophils and monocytes within multiple tissue compartments across time. In patients presenting with acute MI, we observed defined subsets of human peripheral blood neutrophils and monocytes expressing ISGs. In mice, we confirmed these findings and show that ISG expression begins in the bone marrow, is detectable at steady state, is positively regulated by Tet2 in the bone marrow, and is negatively regulated by Nrf2 in resident macrophages of the heart. These data provide comprehensive single cell transcriptomic maps of murine neutrophils, monocytes, and macrophages of the heart, blood, and bone marrow on days 1–4 after MI.

Results

Subsets of peripheral blood monocytes and neutrophils are interferon-stimulated after MI in humans and mice

Healthy human peripheral blood monocytes have been extensively characterized using single cell transcriptomics (24–26); however, it remains unknown whether innate immune signaling pathways are active in trafficking cells at steady-state or after tissue injury. We collected peripheral blood from a patient presenting 48 hours after onset of chest pain with rising serum cardiac troponin levels signifying a non-ST elevation MI (NSTEMI). We collected whole blood, performed red blood cell lysis, and resuspended all of the remaining cells for flow sorting. Cells were stained with DAPI and antibody to cell surface CD235a (glycophorin A), flow sorted to purify live non-doublet non-red blood cells (RBCs), and barcoded using commercial 10X Genomics single cell RNA-seq workflows (Fig. 1A). After demultiplexing and mapping to a reference genome, we performed coarse clustering to broadly define major hematopoietic lineages by expression of canonical markers (fig. 1S). To investigate monocyte heterogeneity, we subset, rescaled, and reclustered $CD14^{HI}VCAN^{HI}FCN1^{HI}$ transcriptomes. This revealed five distinct subpopulations labeled A-E. Cluster A highly expressed several interferon stimulated genes (ISGs): *IFIT1, IFIT2, IFIT3, RSAD2, ISG15, OAS3, RSAD2* (Fig. 1C). Clusters B and C expressed high levels of *CYP1B1, RGS2, ALOX5AP, VNN2, RBP7,* and *S100A9, HMGB2, S100A12, PLBD1, THBS1*, respectively. Clusters D and E expressed high levels of genes associated with dendritic cells (*HLA-DPA, DLA-DPB1)* and were distinguishable by differential expression of *FCGR3A* (also known as CD16) and *FCER1A*. To further investigate interferon stimulation, we constructed a single cell ISG score defined as the summed expression of top ISGs (see Methods). ISG expression was significantly elevated in cells from cluster A compared to clusters B, C, and D, but not compared to dendritic cell cluster E. This is in agreement with Villani et al. (25), which showed that subsets of human dendritic cells also express ISGs.

We next bioinformatically isolated neutrophils defined as $CAMP^{HI}LCN2^{HI}MMP8^{HI}$. Little is known about single cell transcriptomes of human peripheral blood neutrophils because they are commonly discarded by commercial clinical collection tubes. Unbiased sub-clustering of post-MI neutrophils revealed IFN-induced (ISG^{+}) and uninduced (ISG^{-}) populations that spanned the spectrum of maturity (Fig. 1F–H). In mice, we detected analogous subpopulations of ISG^{+} and ISG^{-} neutrophils and monocytes in the post-MO

peripheral blood (Fig. 1I). Taken together, these results suggest that human peripheral blood contains ISG^+ IFN-induced cells (IFNICs) and ISG^- uninduced cells of both neutrophil and monocyte myeloid lineages after MI.

Intracardiac neutrophils are separable into mirrored ISG^+ and ISG^- subsets.

We next directed our attention to the myeloid cells within the infarcted heart. Neutrophils are short-lived first responders to sterile tissue injuries such as MI. In contrast to monocytes and macrophages, little is known about how neutrophils diversify and specialize after entering the injured heart (27, 28). To explore MI-induced heterogeneity, we permanently ligated left coronary arteries and FACS sorted live single non-erythrocytes ($Dapi^{LOW}$, $Ter119^{LOW}$) from flushed and enzymatically digested infarcted hearts on days 1, 2, and 4 (D1, D2, and D4) after MI for single cell RNA-sequencing (fig. S2A,B). Coarse clustering and bioinformatic subsetting of the resulting transcriptomes revealed a neutrophil-predominant distribution on day 1 and a monocyte-macrophage-predominant distribution on day 4 within the infarcted heart consistent with previously reported immunophenotyping and flow cytometry data (fig. S2C–E) (2). We bioinformatically subset neutrophils (*S100a8, S100a9, Retnlg, Mmp9*, *Cxcr2*)^{HI}, renormalized, scaled, and reclustered them both as a unified dataset (Fig. 1) and sample-by-sample (fig. S2). This revealed five intracardiac neutrophil subsets with distinct temporal patterns between D1 and D4 post-MI (Fig. 2A–F, fig. S2, Table S1). The parent neutrophil subset (Hrt-N1*),* characterized by high expression of *Retnlg*, was present in every sample at every time point and phenotypically mirrored peripheral blood neutrophils (Fig. 2A–F, fig. S2, Table S1). Hrt-N2 neutrophils expressed ISGs as early as day 1 after MI and as late as day 4 (Fig. 2A–F, fig. S2, Table S1). This was unexpected since prior work had only uncovered ISG expression within monocyte-derived infarct macrophages (21, 22). We termed these cells neutrophil IFN-induced cells (nIFNICs). The Hrt-N3 subset expressed genes associated with NF-κB activation, including *Nfkb1, Icam1, Il1a, Sod2, and Tnip1* (Fig. 2A–F, fig. S2, Table S1) while the Hrt-N4 population expressed genes associated with HIF-1α activation, including *Egln3, Hilpda, and Vegfa* (Fig. 2A–F, fig. S2, Table S1) *(29)*. Both Hrt-N3 and Hrt-N4 were prominent on day 1 but declined by day 4 in concert with emergence of a new neutrophil subset (Hrt-N5), characterized by expression of *Siglecf* (Fig. 2A–F, fig. S2, Table S1). Although SiglecF is best known as an eosinophil marker and is often gated against when flow sorting neutrophils, recent single cell transcriptomic profiling in the context of murine lung cancer identified a similar SiglecF-expressing neutrophil (30, 31). Indeed, we were able to confirm, using surface antibody staining, that neutrophils ($Cd11b^+$, $Ly6G^+$) are separable into $SiglecF^{HI}$ and $SiglecF^{LOW}$ subpopulations, which allowed FACS sorting and qPCR validation of the single cell RNA-seq findings (fig. S3). These results demonstrate that neutrophils are functionally heterogeneous across time and that $SiglecF^{HI}$ neutrophils may play unrecognized roles within the infarct during late phases of the immune response when remodeling is thought to be dominated by macrophages.

Since we and others previously found type I IFN signaling to be detrimental after MI (21, 22), we inquired whether there were any underlying differences between ISG+ and ISG− neutrophils. Surprisingly, when we bioinformatically isolated and reclustered ISG+ neutrophils, we recovered all of the same inducible neutrophil states present in the ISG− populations (Fig. 2G). To investigate transitions between neutrophil subsets, we performed

pseudotime trajectory analysis (Monocle 3.0) on a down-sampled population of cells (n = 5,000 cells) from post-MI day 4 data (32). Whether analyzed together or individually, ISG^+ and ISG^- neutrophils followed mirrored trajectories (Fig. 2H), reinforcing the view that ISG expression is orthogonal to the other axes of neutrophil differentiation. To examine how ISG expression varies along the neutrophil maturation axis, we compared its expression to *Retnlg* and *Siglecf* (Fig. 2I), which served as markers of early and late intracardiac differentiation. We found that recently infiltrated $Retnlg^{HI}Siglecf^{LOW}$ neutrophils expressed the highest levels of ISGs, suggesting that ISG expression is induced prior to entry into the infarcted heart. Taken together, these results provide the first detailed mapping of neutrophil differentiation within the infarcted heart and show that ISG expression does not limit intracardiac differentiation potential. In addition, these data reveal a previously unrecognized late $Siglecf^+$ neutrophil whose function has yet to be explored.

Intracardiac monocytes and macrophages are separable into mirrored ISG+ and ISG− subsets and one non-mirrored (ISG-) steady-state macrophage subset.

Next, we examined MI-induced intracardiac monocyte and macrophage heterogeneity. We previously found that ISG-expressing monocytes and macrophages in the infarcted heart were dependent on the transcription factor interferon regulatory factor 3 (Irf3) and the type I interferon receptor (Ifnar). Therefore, we induced MI in WT mice as well as $Irf3^{-/-}$, $Ifnar^{-/-}$, and anti-Ifnar antibody treated mice and integrated the resulting single cell transcriptomic datasets (Fig. 3A, fig. S4). We identified six subpopulations of mononuclear cells: Hrt-m1 monocytes (expressing *Ccr2, Plac8,* and *Ms4a4c,* which transcriptionally phenocopy peripheral blood monocytes*)*; an ISG^+ Hrt-m2 population (Hrt-m2); and the following macrophage subsets – Hrt-M3 (expressing *Arg1* and *Vegfa*); Hrt-M4 (expressing *Gclm* and *Slc40a1,* which we later reveal to be Nrf2-activated macrophages); Hrt-M5 (expressing *C1qa C1qb, Mrc1,* and *Ctsd*, including $Ccr2^-$ resident macrophages); and Hrt-M6 (expressing antigen-presenting genes) (Fig. 3B,C, fig. S4A,B,C, Table S2). We termed the ISG^+ Hrt-m2 cells monocyte-derived IFN-induced cells (mIFNICs) to distinguish them from neutrophil IFNICs. Hrt-M5 ($C1qa^{HI}$) and Hrt-M6 ($H2.Aa^{HI}$) were the predominant macrophage subsets of the steady-state heart (Fig. 3D, fig. S4E). When analyzed independently, macrophages from non-infarcted mice subset into $Ccr2^-MHCII^-$, $Ccr2^-MHCII^+$, and $Ccr2^+$ subpopulations, consistent with previous reports (fig. S5A, B)(33). Given their dramatic increases in prevalence from pre- to post-infarction, we inferred that Hrt-m2, -M3, and -M4 were MI-induced states (fig. S4E). ISG-expressing cells from Hrt-m2 (ISG+) represented << 1% of steady-state macrophages yet accounted for ~8% of post-MI mononuclear cells. This population was almost completely absent from the infarcted hearts of anti-Ifnar antibody treated, $Ifnar^{-/-}$, and $Irf3^{-/-}$ mice (Fig. 3E). As an alternative method to clustering, we calculated ISG scores for each cell within each sample, which showed that ISG expression was significantly higher in WT post-MI mononuclear cells compared to pre-infarcted, anti-Ifnar antibody-treated, $Ifnar^{-/-}$ and $Irf3^{-/-}$ mononuclear cells (Fig 3F,G). To explore the differentiation potential of ISG^+ mononuclear cells, we bioinformatically isolated, renormalized, rescaled, and reclustered them. ISG cells spontaneously clustered into the same ISG^- subpopulations with the exception of one uncharacterized macrophage subset, Hrt-M4 (Fig. 3H, fig. S6). Collectively, these data demonstrate that ISGs are induced prior to monocyte arrival to the infarcted heart in an Irf3− and Ifnar-dependent manner. Once in the

heart, ISG^+ and ISG^- monocytes have similar differentiation potentials with the exception of Hrt-M4 macrophages. Because of its unique asymmetry, we turned our attention to the uncharacterized Hrt-M4 macrophages.

MI induces Nrf2-activation in steady-state macrophages, which negatively regulates IFN responses of infiltrating myeloid cells

We noticed that the marker genes of Hrt-M4 were genes previously associated with the cytoprotective transcriptional regulator Nrf2 (Nuclear factor (erythroid-derived 2)-like 2) based on chromatin immunoprecipitation experiments and the presence of Nrf2-binding antioxidant response element (ARE) sequences in their promoters (34–36). To determine whether the Hrt-M4 macrophage population was Nrf2-dependent, we subjected *Nrf2*$^{-/-}$ mice to MI and integrated the resulting single cell transcriptomes with WT pre- and post-infarction data (Fig. 4A,B, fig. S7A,B, Table S3). Indeed, the percentage of Hrt-M4 macrophages decreased from ~12% to <<1% in *Nrf2*$^{-/-}$ mice relative to WT (Fig. 4C, D, fig. S7C–E). Furthermore, differential gene expression analysis comparing *Nrf2*$^{-/-}$ and WT macrophage subsets demonstrated significant reductions in Hrt-M4 cluster-defining genes (Fig. 4E). Based on the abrogation of its marker genes, we concluded that Hrt-M4 cells are Nrf2-activated macrophages and we termed its marker genes Nrf2-stimulated genes (NSGs). Using the top NSGs, we then created a single cell NSG score (analogous to the ISG score above) and confirmed it was significantly reduced in *Nrf2*$^{-/-}$ mice after MI compared to WT (Fig. 4F,G).

Interestingly, NSGs were predominantly expressed in $Ccr2^-$ cells, suggesting that Hrt-M4 macrophages derive from steady-state macrophages rather than recently recruited bone marrow-derived macrophages. To explore this hypothesis, we separately analyzed the single cell transcriptomes of steady-state macrophages and identified four subpopulations as previously reported: *Ccr2*$^-$ *MHCII*$^-$, *Ccr2*$^-$ *MHCII*$^+$, and two *Ccr2*$^+$ subsets (fig. S5A,B)(33). NSG+ (*Hrt-m4*) cells expressed several markers which uniquely defined resident *Ccr2*$^-$ *MHCII*$^-$ macrophages and also closely associated with *Ccr2*$^-$ *MHCII*$^-$ resident macrophages by Spearman's rank coefficient analysis (Fig. 4H, fig. S5B–E). Furthermore, ISGs and NSGs were almost never induced in the same cell (Fig. 4I). Plotting the ISG and NSG scores of single mononuclear cells against each other confirmed the mutually exclusive expression of Irf3− and Nrf2-dependent gene expression programs (Fig. 4J). When placed on a monocyte-to-macrophage differentiation axis using pseudotime trajectory analysis (Monocle), post-MI day 4 Nrf2-induced macrophages associated with mature macrophages, while Irf3-induced cells associated with monocytes (fig. S8). This result was confirmed by flow sorting monocytes and macrophages based on F4/80 and Ly6C surface staining followed by qPCR with primers for highly expressed ISGs and NSGs (Fig. 4K). Taken together, these data suggest that Nrf2-activated Hrt-M4 cells derive from steady-state macrophages and that the ISG-NSG dichotomy is explained by cell location at the time of MI (ISG^+ macrophages derive from monocytes of the blood and bone marrow while NSG^+ macrophages arise from steady-state cells residing within the heart).

Nrf2 negatively regulates inflammation in many models through incompletely-defined mechanisms (37–41). To test whether Nrf2 signaling negatively inhibits expression of ISGs,

we performed mechanistic experiments *in vitro* and *in vivo*. Bone marrow derived macrophages were stimulated with the Irf3-activating cyclic dinucleotide, cyclic-di-GMP (cdGMP), with and without exogenous Nrf2-activating 4-O-itaconate (4OI) (40). Whereas cdGMP alone increased the expression of several ISGs, co-stimulation with cdGMP and 4OI significantly attenuated induction of ISGs while increasing the expression of NSGs (Fig. 4L). *In vivo,* we observed significantly increased levels of ISGs in infarcted Nrf2-deficient mice compared to WT mice as quantified by the ISG score (Fig. 4M), providing further support that ISG expression is Nrf2-dependent after MI. Taken together, these results suggest that Nrf2-activation occurs in $Ccr2^{-}$ steady-state macrophages of the infarcted heart and negatively regulates pathologic ISG expression in infiltrating bone marrow-derived monocytes and neutrophils after MI.

ISGs are expressed in myeloid cells of the murine bone marrow and blood, prior to reaching the infarcted heart.

Since ISG expression was identified in multiple myeloid lineages (neutrophils and monocytes) of the heart, we hypothesized that ISG activation may be initiated within the bone marrow, where myeloid cells arise from a common progenitor (42). To test this, we performed single cell RNA-seq on bone marrow and blood leukocytes and progenitors from infarcted and non-infarcted *WT* and $Irf3^{-/-}$ mice (Fig. 5A, fig. S9, Table S4). After demultiplexing and mapping to a reference genome, transcriptomes were integrated into a single data set and confirmed by examining representation of clusters in independent sample-specific UMAPs (fig. S9A,B). We focused our attention on myeloid progenitors, neutrophils, monocytes (Fig. 5B, fig. S9C). Of the 87,822 total single cell transcriptomes, we measured roughly 40,000 neutrophils and neutrophil progenitors, which spontaneously clustered into 6 continuous subsets (Fig. 5C). By analyzing cluster membership in relation to tissue compartment (i.e. $LS^{+/-}K$ enriched, bone marrow, and blood), we ordered clusters from immature (present only in bone marrow and $LS^{+/-}K$ samples) to mature (present predominantly in blood) (Fig. 5D). We found that ISG expression increased monotonically with neutrophil maturation, beginning at or before the stage of $Camp^{HI}$ neutrophils (Fig. 5E,F). When analyzed at higher resolution (increased dimensionality), ISG^{+} cells spontaneously separated from their parent clusters, and most closely associated with the most mature neutrophils (Fig. 5G). This data demonstrates that the ISG signature is detectable in early neutrophils and intensifies with neutrophil maturation until it becomes a significant component of variability to drive clustering.

We performed a similar analysis for monocytes. In total, 20,295 monocyte transcriptomes were measured, which spontaneously clustered into 5 subsets (Fig. 5H). We ordered monocytes from immature to mature anchored by their relative abundance in the bone marrow and blood. ISG expression was lowest in replicating (*Top2a, Tubb5*)^{HI} and monocyte progenitors (*Fcnb, Cebpe, Ctsg*)^{HI} and monotonically increased in parallel with the production of prototypical monocyte genes (*Lyc2*, *Ccr2*, *Lgals3*) (Fig. 5J–L). When analyzed at higher resolution, ISG^{+} monocytes spontaneously clustered into a distinct subset similar to neutrophils (Fig. 5L).

ISG expression was significantly higher in both neutrophils and monocytes isolated from peripheral blood compared to bone marrow, regardless of time after MI (Fig. 5M). Even at steady-state, we were able to detect ISG^+ myeloid cells in the bone marrow and peripheral blood of uninjured mice. To determine if this finding also applied to humans, we analyzed several previously published studies of healthy human peripheral blood mononuclear cells and found a distinct ISG cluster in four of the six healthy subjects analyzed (URL: https://support.10xgenomics.com/single-cell-gene-expression/datasets) [accessed June 2018]. Whether this is the consequence of an unmeasured environmental stimuli or part of normal hematopoiesis remains unclear (fig. 9S). In mice, whether analyzed at steady state or after MI (D2), the IFN response was Irf3-dependent, as evidenced by significantly decreased expression of ISGs in bone marrow and blood of *Irf3*$^{-/-}$ compared to *WT* mice (Fig. 5N).

The most parsimonious explanation for the observed maturation-dependent ISG expression in mirrored subsets of two myeloid lineages is that activation begins at or before granulocyte-monocyte progenitors (GMP). When we isolated $LS^{+/-}K$ enriched samples, we were unable to detect increased ISG expression in early hematopoietic cells (fig. S9E); however, this does not rule out ISG activation at the GMP stage since cells are maturing as ISG expression is increasing. Rather, a more sensitive assay may be needed to detect the diminutive signal expected at the earliest moments after induction. Nevertheless, our data demonstrates that interferon-induced neutrophils (nIFNICs) and monocytes (mIFNICs) begin far from the site of injury, in the bone marrow, both at steady-state and after MI, and that ISG expression increases with myeloid cell maturation until it becomes distinct enough to elicit spontaneous clustering. Having localized the pro-inflammatory type I IFN response to the bone marrow, we next examined whether an established model of pathologic hyperinflammatory bone marrow may involve alterations in myeloid type I IFN signaling.

Tet2 deficiency increases spontaneous ISG expression in bone marrow myeloid progenitors and their neutrophil and monocyte progeny

Clonal hematopoiesis is an age-associated condition leading to myeloid bias, hyperinflammatory phenotypes, increased risk of cardiovascular events, and increased mortality in humans (43, 44). Loss of function in TET2 (Tet methylcytosine dioxygenase 2), an epigenetic modifier with broad effects on transcription, is one of the most common mutations associated with clonal hematopoiesis in humans. Mechanistic studies of TET2-mutated patients and Tet2-deficient mice have taken a candidate approach and focused on monocyte-derived macrophages, IL-6, IL-1β, and the inflammasome (44–46); however, the importance of other cell types (e.g. neutrophils) and innate immune pathways (e.g. type I IFNs) remains unexplored. We hypothesized that Tet2-deficient mice might have abnormal type I IFN innate immune activation in monocytes and neutrophils of the bone marrow. To test this, we performed single cell RNA-seq of myeloid cells in the bone marrow of *Tet2*$^{-/-}$ mice at steady-state and after MI. Compared to WT mice, we observed heightened and spontaneous induction of ISG expression as quantified by ISG score in myeloid progenitors and their neutrophil and monocyte progeny, both at steady state and after MI (Fig. 6A–D, fig. S10, Table S5). Taken together this data suggests that IFN signaling may be a proinflammatory mediator of Tet2-associated pathology.

Discussion

In summary, our data demonstrate that the type I IFN response to ischemic cardiac injury begins in the bone marrow, far from the site of tissue injury, at the origins of emergency myelopoiesis. We establish that this response occurs not only in monocytes and monocyte-derived macrophages, but also in neutrophils. We show that the type I IFN response is enhanced in the bone marrow of Tet2-deficient mice, is negatively regulated by Nrf2-dependent signaling of $Ccr2^{-}$ steady-state cardiac macrophages, and is Irf3− and Ifnar-dependent (Fig. 7). Our findings have translational significance because the type I IFN response, which was previously thought to be diagnostically inaccessible within the heart, is now readily quantifiable (by calculating single cell ISG scores) in clinically accessible peripheral blood neutrophils and monocytes of patients presenting with acute MI.

Single cell transcriptomics was essential for discrimination of ISG^{+} and ISG^{-} myeloid subpopulations in our study because sensitive and specific antibodies for flow cytometric analysis of this pathway are lacking and because ensemble measurement techniques obscure the relative contributions of individual myeloid cell subsets (47, 48). This functional heterogeneity has pathologic significance because ISGs include many proinflammatory cytokine and chemokine genes (18, 48) and because we previously found that genetic or pharmacologic inhibition of IFN signaling reduces post-MI inflammation and protects against adverse ventricular remodeling and death due to ventricular rupture (21).

Our results raise several mechanistic questions for future studies. How is IFN signaling initiated in subsets of bone marrow myeloid progenitors, and how does it avoid becoming activated in all maturing myeloid cells? Previous studies showed that soluble stimuli such as exogenous poly(I:C) (18, 49) or IFN-α (49), and endogenous IL-1β (50) can induce proliferation of bone marrow stem and progenitor cells, but they were not shown to generate ISG-polarized subsets. It remains unclear how systemic and diffusible substances would activate ISG expression in some, but not all, neutrophils and monocytes. Sympathetic nervous system activation and adrenergic signaling could provide a spatiotemporally localized mechanism for induction, as would proximity to vasculature or another bone marrow niche, but these have not previously been associated with type I IFN signaling or ISG expression (51, 52). Plasmacytoid dendritic cells are involved in tonic IFN signaling (53) and may constitute a bone marrow niche which locally primes myeloid progenitors. We and others observed that ISG expression in the heart was decreased in *Cgas*$^{-/-}$ mice after MI, suggesting that cytosolic DNA sensing may play an important role (21, 22). Irf3-activating signals downstream of cGAS-dependent DNA sensing are gap junction permeable and may mediate contact-dependent intercellular communication (54, 55) with cells of the bone marrow niche (56, 57). Alternatively, cell-autonomous Irf3 activation resulting from DNA damage (58), micronuclei (59, 60), or transient nuclear rupture (61, 62) could generate heterogeneous populations of IFN-induced cells. Finally, identification of heightened spontaneous type I IFN activation in the bone marrow of Tet2-deficient mice suggests IFNs may play an unappreciated role in mediating inflammation in human clonal hematopoiesis (44, 63).

From a clinical perspective, our data provide direct evidence that type I IFN signaling is detectable in peripheral blood neutrophils and monocytes after MI in humans. The ability to quantify ISG expression in peripheral blood leukocyte subsets using single cell transcriptomics will enable correlation with clinical outcomes and response to therapies. Using the single cell ISG score as a biomarker, one can now test whether patients with an excessive type I IFN response to MI are likely to have worse clinical outcomes in terms of arrhythmias, heart failure, recurrent MI, and overall survival. Since we were able to detect ISG^+ myeloid cells in bone marrow and blood of mice at steady state, it will be interesting to compare steady state ISG scores with established inflammatory biomarkers (e.g. C reactive protein) and cardiovascular risk (64, 65). Recent studies have demonstrated that anti-cytokine therapy targeting IL-1β can reduce recurrent cardiovascular events in humans, and it has been suggested that preferential benefit is seen by subsets of patients in whom excessive inflammation drives the pathology (66). Whether quantification of ISG score can identify patients who may preferentially benefit from anti-cytokine or immune modulatory therapy can now be tested. Finally, if ISG scores predict worse outcomes in patients, the causal role of ISGs can be tested using anti-IFNAR antibody therapy, which has shown acceptable safety profiles during chronic administration in a recently reported positive phase 3 clinical trial for lupus (20, 67).

Materials and Methods

Study Design

The aims of this study were to determine the origins and regulatory mechanisms of interferon signaling in myeloid cells at steady-state and after myocardial infarction. We performed single cell RNA-seq on peripheral blood of a human subject presenting with symptoms of MI. We implemented a mouse model of MI to control temporal dynamics and to probe bone marrow and cardiac tissues, which are not readily accessible in human subjects. We used transgenic mice, pharmacological interventions and methods including single cell RNA-seq, flow cytometry, polymerase chain reaction, and in vitro studies to perturb interferon signaling in *in vitro* and *in vivo* models of cardiac injury and inflammation. Experiments were conducted in replicates as indicated in figure legends. No outliers were removed.

Human Study

Peripheral blood was collected from a patient 48 hours after presenting with symptoms of non-ST elevated myocardial infarction (NSTEMI) with a troponin T Gen 5 level of 714 ng/L and a creatine level of 0.71 mg/dL at 12 hours post onset of chest pain. Human material was collected at Sulpizio Cardiovascular Center in association with UC San Diego IRB protocol #140621. Rather than using commercial research collection tubes that isolate peripheral blood mononuclear cells (PBMCs) but discard polynucleated neutrophils, we collected whole blood, performed red blood cell lysis, and resuspended all of the remaining cells for flow sorting. Cells were stained with DAPI and antibody to cell surface CD235a (PE-conjugated HI264; BioLegend), flow sorted to purify live non-doublet non-RBCs, and barcoded using commercial 10X Genomics single cell RNA-seq workflows. Libraries were sequenced on Illumina HiSeq 2500. Sequences were aligned to human genome build

GRCh38 3.0.0, demultiplexed, and filtered using Cell Ranger pipeline (10X Genomics) with standard configurations. The resulting counts matrix was analyzed using R package Seurat v3. We performed recursive unsupervised clustering to first coarsely define major cell lineages and then to examine cell-type specific heterogeneity. ISG were analyzed in publicly available single RNA-seq data sets composed of peripheral blood mononuclear cells from healthy human subjects as indicated in text. Datasets were integrated by projecting PCA structures to reference data, which was selected based on highest ISG expression during independent sample analysis. We increased clustering resolution by increments of 0.1 until an ISG^+ cluster emerged, at which point relative cluster membership was assessed and reported.

Animals

Adult C57BL/6J (*WT,* stock 000664) and Nrf2-deficient mice (stock 017009) mice were purchased from the Jackson Laboratory. $Irf3^{-/-}$ mice (72) were a generous gift from Tadatsugu Taniguchi and provided by Michael Diamond. IFNAR knockout mice ($Ifnar^{-/-}$) were originally from J. Sprent and were backcrossed for 12 generations at the University of Massachusetts Medical School and provided by Kate Fitzgerald. Genotyping was performed in-house using methods recommended by Jackson Laboratory, or by Transnetyx. All experiments were performed with 10 to 14-week-old animals and were carried out using age and gender matched groups without randomization. All mice were maintained in a pathogen-free environment of the UC San Diego or Massachusetts General Hospital animal facilities, and all animal experiments were approved by the Subcommittee on Animal Research Care at UC San Diego or Massachusetts General Hospital.

Myocardial Infarction and IFNAR Antibody Treatment

Mice were intubated and ventilated with 2% isoflurane. After exposing the heart via thoracotomy at the fourth left intercostal space, the left coronary artery was permanently ligated with an 8–0 nylon monofilament suture. The thorax was closed with a 5–0 suture. Mice were treated with buprenorphine for analgesia on the day of surgery and twice daily thereafter for 72 hours. For cardioprotection experiments, mice were treated with two intraperitoneal doses of 500 μg of MAR1–5A3 IFNAR neutralizing antibody (BioXCell) at 8–12 hours and at 48 hours after permanent coronary ligation. Surgeries were performed in a blinded fashion unless genotype was obviated by unavoidable ascertainment of features such as coat color.

Tissue Processing

Bone marrow cells were collected by flushing femurs with ice-cold PBS. The resulting solution was filtered through a 40 μm nylon mesh and treated with RBC lysis buffer (BioLegend). Blood was collected by cardiac puncture. The cellular fraction was collected into EDTA-containing tubes (Sigma), and erythrocytes were eliminated using RBC lysis. Heart tissue was collected by incising the right atrium and perfusing 10 mL of ice-cold saline into the left ventricular apex. Heart tissue was then removed and used for one of several assays detailed below. To obtain single cell suspensions for surface immunostaining, flow cytometric analysis, FACS sorting, or single cell RNA-seq, hearts were enzymatically digested for 1 hour under continuous agitation in 450 U/ml collagenase I, 125 U/ml

collagenase XI, 60 U/ml DNase I, and 60 U/ml hyaluronidase (Sigma) for 1 hour at 37°C, and filtered through a 40 μm nylon mesh cell strainer in FACS buffer (DPBS with 2.5% bovine serum albumin) for enumeration by flow cytometry. For single cell RNA-seq, the enzymatic digestion was limited to 45 minutes to minimize transcript degradation.

Flow cytometry and Cell sorting

Isolated cells from enzymatically digested hearts were stained at 4°C in FACS buffer with DAPI to exclude dead cells, Ter119 (BioLegend, clone TER-119) to remove unlysed red blood cells, and mouse hematopoietic lineage markers directed against B220 (BioLegend, clone RA3–6B2), CD49b (BioLegend, clone DX5), CD90.2 (BioLegend, clone 53–2.1), NK1.1 (BioLegend, clone PK136). Secondary staining of leukocyte subsets was performed using CD45.2 (BioLegend, clone 104), CD11b (BioLegend, clone M1/70), Ly6G (BioLegend, clone 1A8), F4/80 (Biolegend, clone BM8) and/or Ly6C (BioLegend, clone HK1.4 or BD Bioscience, clone AL-21). Neutrophils were identified as (DAPI/B220/CD49b/CD90.2/NK1.1/Ter119)^{low} CD45.2^{high} CD11b^{high} Ly6G^{high}. Monocytes were identified as (DAPI/B220/CD49b/CD90.2/Ly6G/NK1.1/Ter119)^{low} CD45.2^{high} CD11b^{high} and sub-classified as pro-inflammatory monocytes (F4/80^{low}Ly6C^{high}) or macrophages (F4/80^{high}Ly6C$^{low/int}$). Flow cytometry was performed on an LSRII (BD Biosciences), SONY SH800, or SONY MA900, and analyzed with FlowJo software (Tree Star).

Quantitative real-time PCR (qPCR)

Total RNA was extracted from FACS sorted cells or cultured cells using the RNeasy Micro kit (Qiagen) according to the manufacturer's protocol. First-strand cDNA was synthesized using the High-Capacity RNA-to-cDNA kit (Applied Biosystems) according to the manufacturer's instructions. TaqMan gene expression assays (Applied Biosystems) were used to quantify target genes (*Gapdh*: Mm99999915_g1, *Rsad2*: Mm00491265_m1, *Isg15*: Mm01705338_s1, *Isg20*: Mm00469585_m1, *Gclm*: Mm00514996_m1, *Gstm1*: Mm00833915_g1, *Slc40a1*: Mm01254822_m1, *Nqo1*: Mm01253561_m1). Relative changes were normalized to *Gapdh* mRNA using the $2^{-\Delta\Delta CT}$ method.

Single Cell RNA-seq

Single cell RNA-seq was performed by microfluidic droplet-based encapsulation, barcoding, and library preparation, (inDrop and 10X Genomics) as previously described (30). Paired end sequencing was performed on an Illumina HiSeq 2500 and HiSeq 4000 instrument. Low level analysis, including demultiplexing, mapping to a reference transcriptome (Ensembl Release 85 - GRCm38.p5), and eliminating redundant UMIs, was performed according to custom inDrops software (URL: https://github.com/indrops/indrops) [accessed April, 2017] or with CellRanger pipeline for 10X samples.

Single-cell RNA-seq Data Quality Control, Normalization and Integration

To account for variations in sequencing depth, total transcript count for each cell was scaled to 10,000 molecules, and raw counts for each gene were normalized to the total transcript count associated with that cell and then natural log transformed. Cells with between 200 and 2,500 uniquely expressed genes and < 5% mitochondrial counts were retained for further

analysis. Highly variable genes across individual datasets were identified with the *FindVariableFeatures* method from the Seurat R package (version 3.0) by selecting 4,000 genes with the highest feature variance after variance-stabilizing transformation. Integration of multiple single-cell RNA-seq datasets was performed in Seurat to enable harmonized clustering and downstream comparative analyses across conditions(32, 68, 69). Anchoring cell pairs between datasets were identified by Canonical Correlation Analysis (CCA) and the mutual nearest neighbors (MNN) method using the Seurat *FindIntegrationAnchors* function.

Dimensional Reduction, Unsupervised Clustering, Sub-clustering

After scaling and centering expression values for each variable gene, linear dimensionality reduction was performed on integrated data using principal component analysis (PCA). Clustering was performed using the shared nearest neighbor (SNN) clustering algorithm with the Louvain method for modularity optimization, as implemented in the Seurat *FindNeighbors* and *FindClusters* functions. To visualize data in two-dimensional space, Uniform Manifold Approximation and Projection (UMAP) dimensional reduction was performed. Differentially expressed genes between clusters were determined using a Wilcoxon Rank Sum test.

As the highly-variable differentially expressed genes (DEGs) which drive unsupervised clustering are primarily composed of cell-type specific marker genes, we utilized a sub-clustering technique to examine cell-state heterogeneity within cell types in an unbiased manner. This involved serially subsetting particular cell-type clusters, identifying a new set of DEGs within the subset, and re-clustering the subset based on the newly determined DEGs.

Pseudotime

Monocle (v3) package in R was utilized to order cells in pseudotime based on transitional expression patterns within the DEGs (32, 70, 71). Pseudotime trajectories were used to visualize the relationship between cell populations and pseudotime heatmaps were used to determine the dynamics of gene expression patterns in pseudotime. Only genes expressed in greater than 5% of cells were considered for dimensional reduction and differential analysis. For dimensional reduction, the number of dimensions was serially adjusted until branching local minimums were identified. Branching expression analysis modeling was implemented to determine branch dependent gene expression.

ISG and NSG scores

In human samples, ISG scores were measured as the sum of raw reads for the following ISGS: *IFI44L, OAS3, HERC5, IFI6, SAMD9L, IFI44, ISG15, IFIT3, IFIT1, RSAD2, IFIT2, OAS2, EIF2AK2, UBE2L6, SIGLEC1, IFIH1, DDX58, GBP1*. In murine samples, ISG scores were measured as the sum of the raw reads for ten of the top ISGS: *Rsad2*, *Ifit2*, *Ifit3*, *Cmpk2*, *Cxcl10*, *Irf7*, *Isg15*, *Oasl1*, *Mx1*, and *Usp18*. NSG scores were measured as the sum of the raw reads for ten of the top NSGs: *Gclm*, *Slc40a1*, *Gstm1*, *Rnf128*, *Ptgr1*, *Treml4*, *Igf1*, *Cat*, *Ednrb*, and *Cd36*. Both ISG and NSG scores were normalized to reads per cell and scaled by 10^4. ISG product scores were calculated per cell by multiplying ISG scores by the relative abundance of its subset identity as a proportion of total monocytes and macrophages.

The resulting quantities were then averaged within each subset and displayed as a single score per subset per mouse.

Spearman's Rank Correlation Coefficients

Intracardiac neutrophil subsets were averaged and ranked by subset defining DEGs (scaled data) to create a comparator ranked gene list. A Spearman's rank correlation coefficient (ρ) for each cell was calculated by $\rho = \frac{1 - 6\sum d_i^2}{n(n^2 - 1)}$ (where d is the distance between gene ranks, n is number of genes) and averaged within subsets.

Bone Marrow Derived Macrophage Stimulation

For *in vitro* stimulation, cyclic-di-GMP (Invivogen) (10ug/mL of media) and 4-octyl-itaconate (Tocris Bioscience) (100 μM) were added to each well of a 6-well plate. After 24 hours of stimulation, RNA was extracted and quantified by qPCR as above.

Statistics

Statistical analysis was performed using GraphPad Prism software. All data are represented as mean values +/− standard error of mean (S.E.M.) unless indicated otherwise. A statistical method was not used to predetermine sample size. For comparisons of the qPCR data and ISG/NSG scores, a 2-tailed t-test with Welch's correction was to determine statistical significance. All analyses were unpaired. *P* values are indicated by *P* values less than 0.05 were considered significant and are indicated by asterisks as follows: *p<0.05, **p<0.01, ***p<0.001, ****p<0.0001.

Supplementary Material

Refer to Web version on PubMed Central for supplementary material.

Acknowledgements.

We thank the Single Cell Core at Harvard Medical School and the Institute of Genomic Medicine at UC San Diego for technical assistance.

Funding. The work was funded by NIH grants UL1TR001442 (UCSD); AHA17IRG33410543 (K.R.K), NIH R00HL129168 (K.R.K.), and DP2AR075321 (K.R.K.); AHA14FTF20380185 (A.D.A.) and NIH R01HL144515 (A.D.A); 5R01HL122208 (R.W.), R01CA206890 (R.W), and R01HL131495 (R.W.); and NIH T32HL105373 (D.M.C).

References and Notes

1. G. B. D. C. o. D. Collaborators, Global, regional, and national age-sex-specific mortality for 282 causes of death in 195 countries and territories, 1980–2017: a systematic analysis for the Global Burden of Disease Study 2017. Lancet 392, 1736–1788 (2018). [PubMed: 30496103]
2. Nahrendorf M, Swirski FK, Aikawa E, Stangenberg L, Wurdinger T, Figueiredo JL, Libby P, Weissleder R, Pittet MJ, The healing myocardium sequentially mobilizes two monocyte subsets with divergent and complementary functions. J Exp Med 204, 3037–3047 (2007). [PubMed: 18025128]
3. Boettcher S, Manz MG, Sensing and translation of pathogen signals into demand-adapted myelopoiesis. Curr Opin Hematol 23, 5–10 (2016). [PubMed: 26554891]

4. Dutta P, Sager HB, Stengel KR, Naxerova K, Courties G, Saez B, Silberstein L, Heidt T, Sebas M, Sun Y, Wojtkiewicz G, Feruglio PF, King K, Baker JN, van der Laan AM, Borodovsky A, Fitzgerald K, Hulsmans M, Hoyer F, Iwamoto Y, Vinegoni C, Brown D, Di Carli M, Libby P, Hiebert SW, Scadden DT, Swirski FK, Weissleder R, Nahrendorf M, Myocardial Infarction Activates CCR2(+) Hematopoietic Stem and Progenitor Cells. Cell Stem Cell 16, 477–487 (2015). [PubMed: 25957903]
5. Herault A, Binnewies M, Leong S, Calero-Nieto FJ, Zhang SY, Kang YA, Wang X, Pietras EM, Chu SH, Barry-Holson K, Armstrong S, Gottgens B, Passegue E, Myeloid progenitor cluster formation drives emergency and leukaemic myelopoiesis. Nature 544, 53–58 (2017). [PubMed: 28355185]
6. Manz MG, Boettcher S, Emergency granulopoiesis. Nat Rev Immunol 14, 302–314 (2014). [PubMed: 24751955]
7. Hoyer FF, Naxerova K, Schloss MJ, Hulsmans M, Nair AV, Dutta P, Calcagno DM, Herisson F, Anzai A, Sun Y, Wojtkiewicz G, Rohde D, Frodermann V, Vandoorne K, Courties G, Iwamoto Y, Garris CS, Williams DL, Breton S, Brown D, Whalen M, Libby P, Pittet MJ, King KR, Weissleder R, Swirski FK, Nahrendorf M, Tissue-Specific Macrophage Responses to Remote Injury Impact the Outcome of Subsequent Local Immune Challenge. Immunity 51, 899–914 e897 (2019).
8. Vinten-Johansen J, Involvement of neutrophils in the pathogenesis of lethal myocardial reperfusion injury. Cardiovasc Res 61, 481–497 (2004). [PubMed: 14962479]
9. Puhl SL, Steffens S, Neutrophils in Post-myocardial Infarction Inflammation: Damage vs. Resolution? Front Cardiovasc Med 6, 25 (2019). [PubMed: 30937305]
10. Horckmans M, Ring L, Duchene J, Santovito D, Schloss MJ, Drechsler M, Weber C, Soehnlein O, Steffens S, Neutrophils orchestrate post-myocardial infarction healing by polarizing macrophages towards a reparative phenotype. Eur Heart J 38, 187–197 (2017). [PubMed: 28158426]
11. Granger DN, Korthuis RJ, Physiologic mechanisms of postischemic tissue injury. Annu Rev Physiol 57, 311–332 (1995). [PubMed: 7778871]
12. Leuschner F, Rauch PJ, Ueno T, Gorbatov R, Marinelli B, Lee WW, Dutta P, Wei Y, Robbins C, Iwamoto Y, Sena B, Chudnovskiy A, Panizzi P, Keliher E, Higgins JM, Libby P, Moskowitz MA, Pittet MJ, Swirski FK, Weissleder R, Nahrendorf M, Rapid monocyte kinetics in acute myocardial infarction are sustained by extramedullary monocytopoiesis. J Exp Med 209, 123–137 (2012). [PubMed: 22213805]
13. Epelman S, Lavine KJ, Beaudin AE, Sojka DK, Carrero JA, Calderon B, Brija T, Gautier EL, Ivanov S, Satpathy AT, Schilling JD, Schwendener R, Sergin I, Razani B, Forsberg EC, Yokoyama WM, Unanue ER, Colonna M, Randolph GJ, Mann DL, Embryonic and adult-derived resident cardiac macrophages are maintained through distinct mechanisms at steady state and during inflammation. Immunity 40, 91–104 (2014). [PubMed: 24439267]
14. Dick SA, Macklin JA, Nejat S, Momen A, Clemente-Casares X, Althagafi MG, Chen J, Kantores C, Hosseinzadeh S, Aronoff L, Wong A, Zaman R, Barbu I, Besla R, Lavine KJ, Razani B, Ginhoux F, Husain M, Cybulsky MI, Robbins CS, Epelman S, Self-renewing resident cardiac macrophages limit adverse remodeling following myocardial infarction. Nat Immunol 20, 29–39 (2019). [PubMed: 30538339]
15. Bajpai G, Bredemeyer A, Li W, Zaitsev K, Koenig AL, Lokshina I, Mohan J, Ivey B, Hsiao HM, Weinheimer C, Kovacs A, Epelman S, Artyomov M, Kreisel D, Lavine KJ, Tissue Resident CCR2− and CCR2+ Cardiac Macrophages Differentially Orchestrate Monocyte Recruitment and Fate Specification Following Myocardial Injury. Circ Res 124, 263–278 (2019). [PubMed: 30582448]
16. Kaczmarek A, Vandenabeele P, Krysko DV, Necroptosis: the release of damage-associated molecular patterns and its physiological relevance. Immunity 38, 209–223 (2013). [PubMed: 23438821]
17. Arslan F, de Kleijn DP, Pasterkamp G, Innate immune signaling in cardiac ischemia. Nat Rev Cardiol 8, 292–300 (2011). [PubMed: 21448140]
18. Muller U, Steinhoff U, Reis LF, Hemmi S, Pavlovic J, Zinkernagel RM, Aguet M, Functional role of type I and type II interferons in antiviral defense. Science 264, 1918–1921 (1994). [PubMed: 8009221]
19. Lee-Kirsch MA, The Type I Interferonopathies. Annu Rev Med 68, 297–315 (2017). [PubMed: 27813875]

20. Furie R, Khamashta M, Merrill JT, Werth VP, Kalunian K, Brohawn P, Illei GG, Drappa J, Wang L, Yoo S, Investigators CDS, Anifrolumab, an Anti-Interferon-alpha Receptor Monoclonal Antibody, in Moderate-to-Severe Systemic Lupus Erythematosus. Arthritis Rheumatol 69, 376–386 (2017). [PubMed: 28130918]
21. King KR, Aguirre AD, Ye YX, Sun Y, Roh JD, Ng RP Jr., Kohler RH, Arlauckas SP, Iwamoto Y, Savol A, Sadreyev RI, Kelly M, Fitzgibbons TP, Fitzgerald KA, Mitchison T, Libby P, Nahrendorf M, Weissleder R, IRF3 and type I interferons fuel a fatal response to myocardial infarction. Nat Med 23, 1481–1487 (2017). [PubMed: 29106401]
22. Cao DJ, Schiattarella GG, Villalobos E, Jiang N, May HI, Li T, Chen ZJ, Gillette TG, Hill JA, Cytosolic DNA Sensing Promotes Macrophage Transformation and Governs Myocardial Ischemic Injury. Circulation 137, 2613–2634 (2018). [PubMed: 29437120]
23. Zilionis R, Nainys J, Veres A, Savova V, Zemmour D, Klein AM, Mazutis L, Single-cell barcoding and sequencing using droplet microfluidics. Nat Protoc 12, 44–73 (2017). [PubMed: 27929523]
24. Zheng GX, Terry JM, Belgrader P, Ryvkin P, Bent ZW, Wilson R, Ziraldo SB, Wheeler TD, McDermott GP, Zhu J, Gregory MT, Shuga J, Montesclaros L, Underwood JG, Masquelier DA, Nishimura SY, Schnall-Levin M, Wyatt PW, Hindson CM, Bharadwaj R, Wong A, Ness KD, Beppu LW, Deeg HJ, McFarland C, Loeb KR, Valente WJ, Ericson NG, Stevens EA, Radich JP, Mikkelsen TS, Hindson BJ, Bielas JH, Massively parallel digital transcriptional profiling of single cells. Nat Commun 8, 14049 (2017). [PubMed: 28091601]
25. Villani AC, Satija R, Reynolds G, Sarkizova S, Shekhar K, Fletcher J, Griesbeck M, Butler A, Zheng S, Lazo S, Jardine L, Dixon D, Stephenson E, Nilsson E, Grundberg I, McDonald D, Filby A, Li W, De Jager PL, Rozenblatt-Rosen O, Lane AA, Haniffa M, Regev A, Hacohen N, Single-cell RNA-seq reveals new types of human blood dendritic cells, monocytes, and progenitors. Science 356, (2017).
26. Han X, Wang R, Zhou Y, Fei L, Sun H, Lai S, Saadatpour A, Zhou Z, Chen H, Ye F, Huang D, Xu Y, Huang W, Jiang M, Jiang X, Mao J, Chen Y, Lu C, Xie J, Fang Q, Wang Y, Yue R, Li T, Huang H, Orkin SH, Yuan GC, Chen M, Guo G, Mapping the Mouse Cell Atlas by Microwell-Seq. Cell 173, 1307 (2018). [PubMed: 29775597]
27. Ng LG, Ostuni R, Hidalgo A, Heterogeneity of neutrophils. Nat Rev Immunol 19, 255–265 (2019). [PubMed: 30816340]
28. Silvestre-Roig C, Hidalgo A, Soehnlein O, Neutrophil heterogeneity: implications for homeostasis and pathogenesis. Blood 127, 2173–2181 (2016). [PubMed: 27002116]
29. Walmsley SR, Chilvers ER, Thompson AA, Vaughan K, Marriott HM, Parker LC, Shaw G, Parmar S, Schneider M, Sabroe I, Dockrell DH, Milo M, Taylor CT, Johnson RS, Pugh CW, Ratcliffe PJ, Maxwell PH, Carmeliet P, Whyte MK, Prolyl hydroxylase 3 (PHD3) is essential for hypoxic regulation of neutrophilic inflammation in humans and mice. J Clin Invest 121, 1053–1063 (2011). [PubMed: 21317538]
30. Engblom C, Pfirschke C, Zilionis R, Da Silva Martins J, Bos SA, Courties G, Rickelt S, Severe N, Baryawno N, Faget J, Savova V, Zemmour D, Kline J, Siwicki M, Garris C, Pucci F, Liao HW, Lin YJ, Newton A, Yaghi OK, Iwamoto Y, Tricot B, Wojtkiewicz GR, Nahrendorf M, Cortez-Retamozo V, Meylan E, Hynes RO, Demay M, Klein A, Bredella MA, Scadden DT, Weissleder R, Pittet MJ, Osteoblasts remotely supply lung tumors with cancer-promoting SiglecF(high) neutrophils. Science 358, (2017).
31. Zilionis R, Engblom C, Pfirschke C, Savova V, Zemmour D, Saatcioglu HD, Krishnan I, Maroni G, Meyerovitz CV, Kerwin CM, Choi S, Richards WG, De Rienzo A, Tenen DG, Bueno R, Levantini E, Pittet MJ, Klein AM, Single-Cell Transcriptomics of Human and Mouse Lung Cancers Reveals Conserved Myeloid Populations across Individuals and Species. Immunity 50, 1317–1334 e1310 (2019).
32. Qiu X, Mao Q, Tang Y, Wang L, Chawla R, Pliner HA, Trapnell C, Reversed graph embedding resolves complex single-cell trajectories. Nat Methods 14, 979–982 (2017). [PubMed: 28825705]
33. Dick SA, Epelman S, Chronic Heart Failure and Inflammation: What Do We Really Know? Circ Res 119, 159–176 (2016). [PubMed: 27340274]
34. Moi P, Chan K, Asunis I, Cao A, Kan YW, Isolation of NF-E2-related factor 2 (Nrf2), a NF-E2-like basic leucine zipper transcriptional activator that binds to the tandem NF-E2/AP1 repeat of the

beta-globin locus control region. Proc Natl Acad Sci U S A 91, 9926–9930 (1994). [PubMed: 7937919]

35. Malhotra D, Portales-Casamar E, Singh A, Srivastava S, Arenillas D, Happel C, Shyr C, Wakabayashi N, Kensler TW, Wasserman WW, Biswal S, Global mapping of binding sites for Nrf2 identifies novel targets in cell survival response through ChIP-Seq profiling and network analysis. Nucleic Acids Res 38, 5718–5734 (2010). [PubMed: 20460467]
36. Lee JM, Calkins MJ, Chan K, Kan YW, Johnson JA, Identification of the NF-E2-related factor-2-dependent genes conferring protection against oxidative stress in primary cortical astrocytes using oligonucleotide microarray analysis. J Biol Chem 278, 12029–12038 (2003). [PubMed: 12556532]
37. Lee JM, Li J, Johnson DA, Stein TD, Kraft AD, Calkins MJ, Jakel RJ, Johnson JA, Nrf2, a multi-organ protector? FASEB J 19, 1061–1066 (2005). [PubMed: 15985529]
38. Thimmulappa RK, Lee H, Rangasamy T, Reddy SP, Yamamoto M, Kensler TW, Biswal S, Nrf2 is a critical regulator of the innate immune response and survival during experimental sepsis. J Clin Invest 116, 984–995 (2006). [PubMed: 16585964]
39. Ahmed SM, Luo L, Namani A, Wang XJ, Tang X, Nrf2 signaling pathway: Pivotal roles in inflammation. Biochim Biophys Acta Mol Basis Dis 1863, 585–597 (2017). [PubMed: 27825853]
40. Mills EL, Ryan DG, Prag HA, Dikovskaya D, Menon D, Zaslona Z, Jedrychowski MP, Costa ASH, Higgins M, Hams E, Szpyt J, Runtsch MC, King MS, McGouran JF, Fischer R, Kessler BM, McGettrick AF, Hughes MM, Carroll RG, Booty LM, Knatko EV, Meakin PJ, Ashford MLJ, Modis LK, Brunori G, Sevin DC, Fallon PG, Caldwell ST, Kunji ERS, Chouchani ET, Frezza C, Dinkova-Kostova AT, Hartley RC, Murphy MP, O'Neill LA, Itaconate is an anti-inflammatory metabolite that activates Nrf2 via alkylation of KEAP1. Nature 556, 113–117 (2018). [PubMed: 29590092]
41. Yu XH, Zhang DW, Zheng XL, Tang CK, Itaconate: an emerging determinant of inflammation in activated macrophages. Immunol Cell Biol 97, 134–141 (2019). [PubMed: 30428148]
42. Schultze JL, Mass E, Schlitzer A, Emerging Principles in Myelopoiesis at Homeostasis and during Infection and Inflammation. Immunity 50, 288–301 (2019). [PubMed: 30784577]
43. Jaiswal S, Fontanillas P, Flannick J, Manning A, Grauman PV, Mar BG, Lindsley RC, Mermel CH, Burtt N, Chavez A, Higgins JM, Moltchanov V, Kuo FC, Kluk MJ, Henderson B, Kinnunen L, Koistinen HA, Ladenvall C, Getz G, Correa A, Banahan BF, Gabriel S, Kathiresan S, Stringham HM, McCarthy MI, Boehnke M, Tuomilehto J, Haiman C, Groop L, Atzmon G, Wilson JG, Neuberg D, Altshuler D, Ebert BL, Age-related clonal hematopoiesis associated with adverse outcomes. N Engl J Med 371, 2488–2498 (2014). [PubMed: 25426837]
44. Jaiswal S, Natarajan P, Silver AJ, Gibson CJ, Bick AG, Shvartz E, McConkey M, Gupta N, Gabriel S, Ardissino D, Baber U, Mehran R, Fuster V, Danesh J, Frossard P, Saleheen D, Melander O, Sukhova GK, Neuberg D, Libby P, Kathiresan S, Ebert BL, Clonal Hematopoiesis and Risk of Atherosclerotic Cardiovascular Disease. N Engl J Med 377, 111–121 (2017). [PubMed: 28636844]
45. Fuster JJ, MacLauchlan S, Zuriaga MA, Polackal MN, Ostriker AC, Chakraborty R, Wu CL, Sano S, Muralidharan S, Rius C, Vuong J, Jacob S, Muralidhar V, Robertson AA, Cooper MA, Andres V, Hirschi KK, Martin KA, Walsh K, Clonal hematopoiesis associated with TET2 deficiency accelerates atherosclerosis development in mice. Science 355, 842–847 (2017). [PubMed: 28104796]
46. Bick AG, Pirruccello JP, Griffin GK, Gupta N, Gabriel S, Saleheen D, Libby P, Kathiresan S, Natarajan P, Genetic IL-6 Signaling Deficiency Attenuates Cardiovascular Risk in Clonal Hematopoiesis. Circulation, (2019).
47. Shalek AK, Satija R, Adiconis X, Gertner RS, Gaublomme JT, Raychowdhury R, Schwartz S, Yosef N, Malboeuf C, Lu D, Trombetta JJ, Gennert D, Gnirke A, Goren A, Hacohen N, Levin JZ, Park H, Regev A, Single-cell transcriptomics reveals bimodality in expression and splicing in immune cells. Nature 498, 236–240 (2013). [PubMed: 23685454]
48. Shalek AK, Satija R, Shuga J, Trombetta JJ, Gennert D, Lu D, Chen P, Gertner RS, Gaublomme JT, Yosef N, Schwartz S, Fowler B, Weaver S, Wang J, Wang X, Ding R, Raychowdhury R, Friedman N, Hacohen N, Park H, May AP, Regev A, Single-cell RNA-seq reveals dynamic paracrine control of cellular variation. Nature 510, 363–369 (2014). [PubMed: 24919153]

49. Essers MA, Offner S, Blanco-Bose WE, Waibler Z, Kalinke U, Duchosal MA, Trumpp A, IFNalpha activates dormant haematopoietic stem cells in vivo. Nature 458, 904–908 (2009). [PubMed: 19212321]
50. Sager HB, Heidt T, Hulsmans M, Dutta P, Courties G, Sebas M, Wojtkiewicz GR, Tricot B, Iwamoto Y, Sun Y, Weissleder R, Libby P, Swirski FK, Nahrendorf M, Targeting Interleukin-1beta Reduces Leukocyte Production After Acute Myocardial Infarction. Circulation 132, 1880–1890 (2015). [PubMed: 26358260]
51. Katayama Y, Battista M, Kao WM, Hidalgo A, Peired AJ, Thomas SA, Frenette PS, Signals from the sympathetic nervous system regulate hematopoietic stem cell egress from bone marrow. Cell 124, 407–421 (2006). [PubMed: 16439213]
52. Dutta P, Courties G, Wei Y, Leuschner F, Gorbatov R, Robbins CS, Iwamoto Y, Thompson B, Carlson AL, Heidt T, Majmudar MD, Lasitschka F, Etzrodt M, Waterman P, Waring MT, Chicoine AT, van der Laan AM, Niessen HW, Piek JJ, Rubin BB, Butany J, Stone JR, Katus HA, Murphy SA, Morrow DA, Sabatine MS, Vinegoni C, Moskowitz MA, Pittet MJ, Libby P, Lin CP, Swirski FK, Weissleder R, Nahrendorf M, Myocardial infarction accelerates atherosclerosis. Nature 487, 325–329 (2012). [PubMed: 22763456]
53. Schaupp L, Muth S, Rogell L, Kofoed-Branzk M, Melchior F, Lienenklaus S, Ganal-Vonarburg SC, Klein M, Guendel F, Hain T, Schutze K, Grundmann U, Schmitt V, Dorsch M, Spanier J, Larsen PK, Schwanz T, Jackel S, Reinhardt C, Bopp T, Danckwardt S, Mahnke K, Heinz GA, Mashreghi MF, Durek P, Kalinke U, Kretz O, Huber TB, Weiss S, Wilhelm C, Macpherson AJ, Schild H, Diefenbach A, Probst HC, Microbiota-Induced Type I Interferons Instruct a Poised Basal State of Dendritic Cells. Cell 181, 1080–1096 e1019 (2020).
54. Patel SJ, King KR, Casali M, Yarmush ML, DNA-triggered innate immune responses are propagated by gap junction communication. Proc Natl Acad Sci U S A 106, 12867–12872 (2009). [PubMed: 19617563]
55. Ablasser A, Schmid-Burgk JL, Hemmerling I, Horvath GL, Schmidt T, Latz E, Hornung V, Cell intrinsic immunity spreads to bystander cells via the intercellular transfer of cGAMP. Nature 503, 530–534 (2013). [PubMed: 24077100]
56. Pinho S, Frenette PS, Haematopoietic stem cell activity and interactions with the niche. Nat Rev Mol Cell Biol 20, 303–320 (2019). [PubMed: 30745579]
57. Tikhonova AN, Dolgalev I, Hu H, Sivaraj KK, Hoxha E, Cuesta-Dominguez A, Pinho S, Akhmetzyanova I, Gao J, Witkowski M, Guillamot M, Gutkin MC, Zhang Y, Marier C, Diefenbach C, Kousteni S, Heguy A, Zhong H, Fooksman DR, Butler JM, Economides A, Frenette PS, Adams RH, Satija R, Tsirigos A, Aifantis I, The bone marrow microenvironment at single-cell resolution. Nature 569, 222–228 (2019). [PubMed: 30971824]
58. Li T, Chen ZJ, The cGAS-cGAMP-STING pathway connects DNA damage to inflammation, senescence, and cancer. J Exp Med 215, 1287–1299 (2018). [PubMed: 29622565]
59. Harding SM, Benci JL, Irianto J, Discher DE, Minn AJ, Greenberg RA, Mitotic progression following DNA damage enables pattern recognition within micronuclei. Nature 548, 466–470 (2017). [PubMed: 28759889]
60. Mackenzie KJ, Carroll P, Martin CA, Murina O, Fluteau A, Simpson DJ, Olova N, Sutcliffe H, Rainger JK, Leitch A, Osborn RT, Wheeler AP, Nowotny M, Gilbert N, Chandra T, Reijns MAM, Jackson AP, cGAS surveillance of micronuclei links genome instability to innate immunity. Nature 548, 461–465 (2017). [PubMed: 28738408]
61. Denais CM, Gilbert RM, Isermann P, McGregor AL, te Lindert M, Weigelin B, Davidson PM, Friedl P, Wolf K, Lammerding J, Nuclear envelope rupture and repair during cancer cell migration. Science 352, 353–358 (2016). [PubMed: 27013428]
62. Raab M, Gentili M, de Belly H, Thiam HR, Vargas P, Jimenez AJ, Lautenschlaeger F, Voituriez R, Lennon-Dumenil AM, Manel N, Piel M, ESCRT III repairs nuclear envelope ruptures during cell migration to limit DNA damage and cell death. Science 352, 359–362 (2016). [PubMed: 27013426]
63. Jaiswal S, Natarajan P, Ebert BL, Clonal Hematopoiesis and Atherosclerosis. N Engl J Med 377, 1401–1402 (2017).

64. Ridker PM, High-sensitivity C-reactive protein, inflammation, and cardiovascular risk: from concept to clinical practice to clinical benefit. Am Heart J 148, S19–26 (2004). [PubMed: 15211329]

65. Ridker PM, Hennekens CH, Buring JE, Rifai N, C-reactive protein and other markers of inflammation in the prediction of cardiovascular disease in women. N Engl J Med 342, 836–843 (2000). [PubMed: 10733371]

66. Ridker PM, Everett BM, Thuren T, MacFadyen JG, Chang WH, Ballantyne C, Fonseca F, Nicolau J, Koenig W, Anker SD, Kastelein JJP, Cornel JH, Pais P, Pella D, Genest J, Cifkova R, Lorenzatti A, Forster T, Kobalava Z, Vida-Simiti L, Flather M, Shimokawa H, Ogawa H, Dellborg M, Rossi PRF, Troquay RPT, Libby P, Glynn RJ, Group CT, Antiinflammatory Therapy with Canakinumab for Atherosclerotic Disease. N Engl J Med 377, 1119–1131 (2017). [PubMed: 28845751]

67. Morand EF, Furie R, Tanaka Y, Bruce IN, Askanase AD, Richez C, Bae SC, Brohawn PZ, Pineda L, Berglind A, Tummala R, Investigators T-T, Trial of Anifrolumab in Active Systemic Lupus Erythematosus. N Engl J Med 382, 211–221 (2020). [PubMed: 31851795]

68. Stuart T, Butler A, Hoffman P, Hafemeister C, Papalexi E, Mauck WM 3rd, Hao Y, Stoeckius M, Smibert P, Satija R, Comprehensive Integration of Single-Cell Data. Cell 177, 1888–1902 e1821 (2019).

69. Butler A, Hoffman P, Smibert P, Papalexi E, Satija R, Integrating single-cell transcriptomic data across different conditions, technologies, and species. Nat Biotechnol 36, 411–420 (2018). [PubMed: 29608179]

70. Qiu X, Hill A, Packer J, Lin D, Ma YA, Trapnell C, Single-cell mRNA quantification and differential analysis with Census. Nat Methods 14, 309–315 (2017). [PubMed: 28114287]

71. Trapnell C, Cacchiarelli D, Grimsby J, Pokharel P, Li S, Morse M, Lennon NJ, Livak KJ, Mikkelsen TS, Rinn JL, The dynamics and regulators of cell fate decisions are revealed by pseudotemporal ordering of single cells. Nat Biotechnol 32, 381–386 (2014). [PubMed: 24658644]

72. Sato M, Suemori H, Hata N. et al. Distinct and essential roles of transcription factors IRF-3 and IRF-7 in response to viruses for IFN-alpha/beta gene induction. Immunity 13, 539–548 (2000). [PubMed: 11070172] (** This reference was a late addition to the Methods and is known to be out of order).

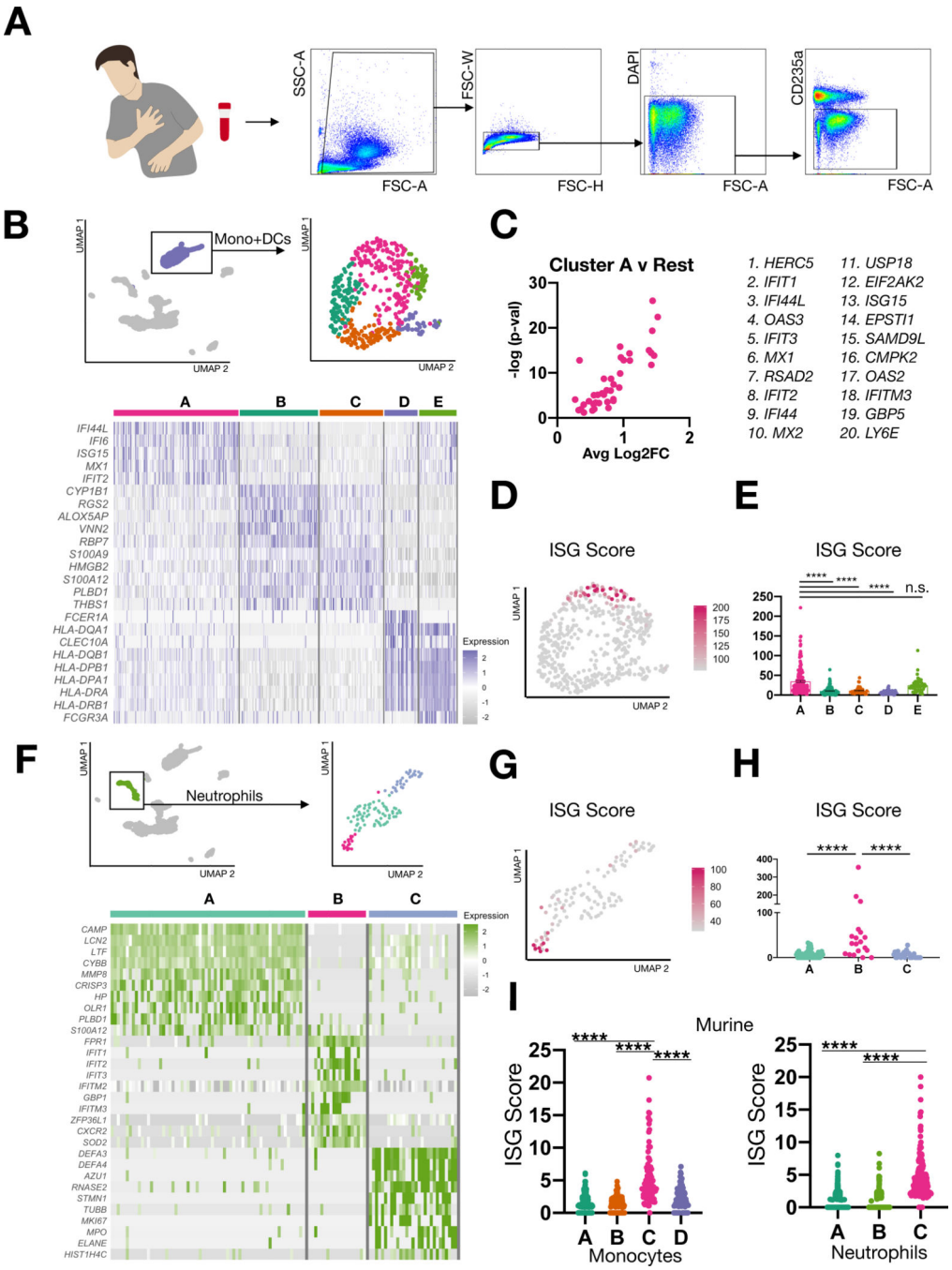

Figure 1. ISG expression in peripheral blood myeloid cells of humans and mice after MI.

(**A**) Peripheral blood from an NSTEMI patient (714 ng/L Troponin T Gen 5 at 12 hrs post onset-time) was collected 28 hours post-onset and FACS sorted for 10X Genomics single cell RNA-sequencing (n = 3,102 cells). (**B**) UMAP and heatmap of bioinformatically isolated and reclustered mononuclear cells (n = 468 cells). (**C**) Volcano plot of top differential expressed genes (Wilcoxon Rank Sums test) in cluster A versus rest of clusters. All genes shown had significant (< 0.001) Bonferroni corrected p-values. (**D,E**) ISG scores, defined as the summed expression of top ISGs (see methods), were calculated for each cell

and shown by intensity on UMAP (**D**) and by cluster (**E**). (**F**) UMAP and heatmap of bioinformatically isolated and reclustered neutrophils. (**G,H**) ISG score shown by intensity on neutrophil UMAP (n = 112 cells) (**G**), and by subset (**H**). (**I**) ISG score of subclustered murine peripheral blood monocytes and neutrophils on D4 (n = 532 cells), and D1 (n = 2,651 cells) post-MI, respectively. **** P< 0.0001, Mann-Whitney test.

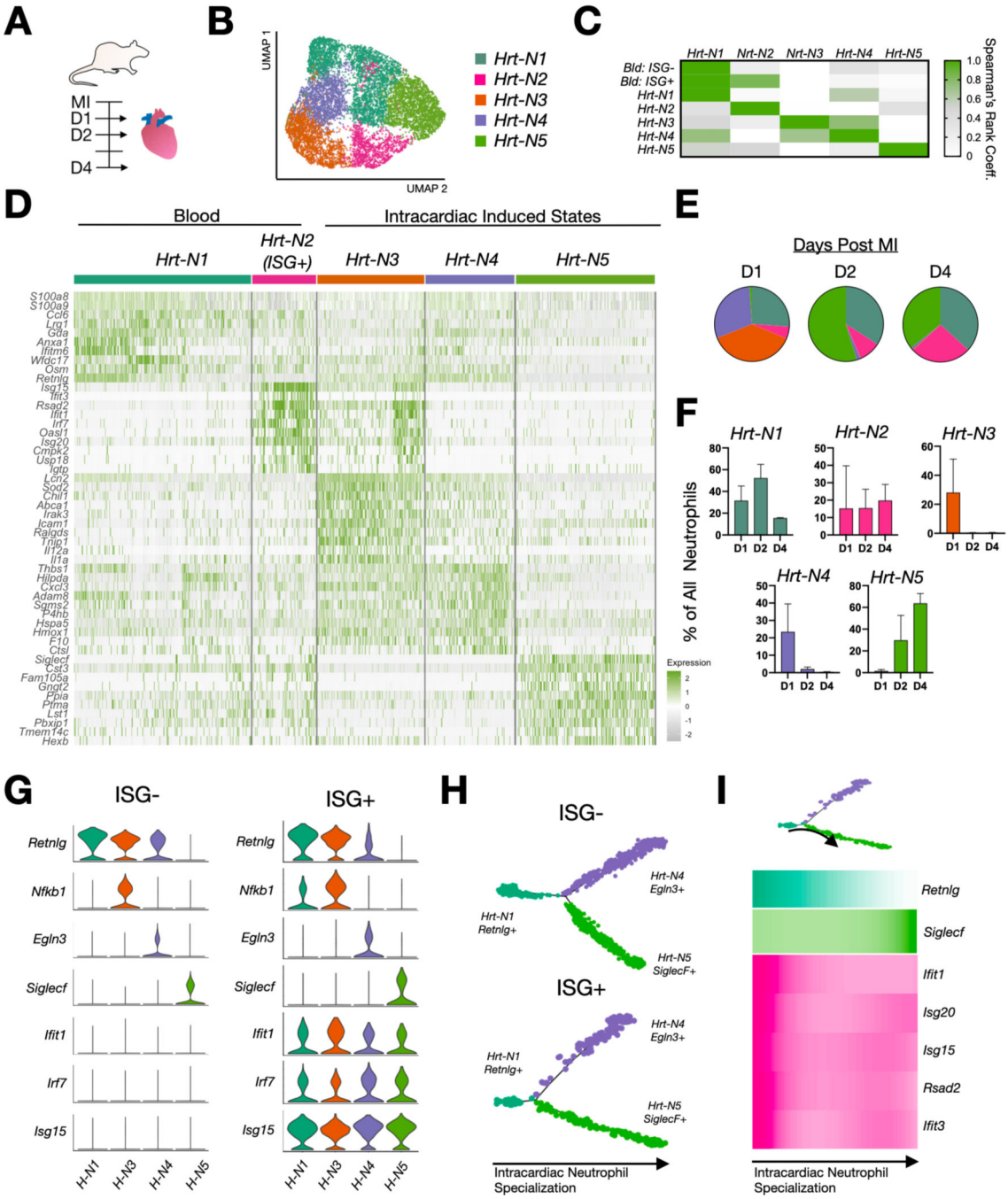

Figure 2. Intracardiac neutrophils are separable into mirrored ISG+ and ISG− subsets within the infarcted mouse heart.

(**A**) Infarcted hearts D1, D2, and D4 after MI were enzymatically digested, FACS sorted (singlets, DAPI^{-}Ter119^{-}) and barcoded for single cell RNA sequencing using custom inDrop barcoding platform (N = 3 biological replicates per day post-MI; 10,666 cells). (**B**) UMAP of bioinformatically isolated and integrated neutrophils (*S100a8, S100a9, Cxcr2, Csf3r*)^{HI}. (**C**) Spearman's rank correlation coefficient comparing heart and blood neutrophil subsets. (**D**) Integrated heatmap. (**E,F**) Distribution of neutrophil subsets by time (data are

shown as mean +/− S.E.M). (**G**) Violin plots of subclustered ISG^{-} and ISG^{+} cells (D1, D2 and D4 post-MI combined). Top marker gene for each neutrophil subset shown. (**H**, **I**) Pseudotime trajectory (Monocle) on ISG^{-} and ISG^{+} (**H**) and heatmap of neutrophil maturation and ISG expression vs pseudotime (**I**) from $Retnlg^{HI}Siglecf^{LOW}$ to $Retnlg^{LOW}Siglecf^{HI}$.

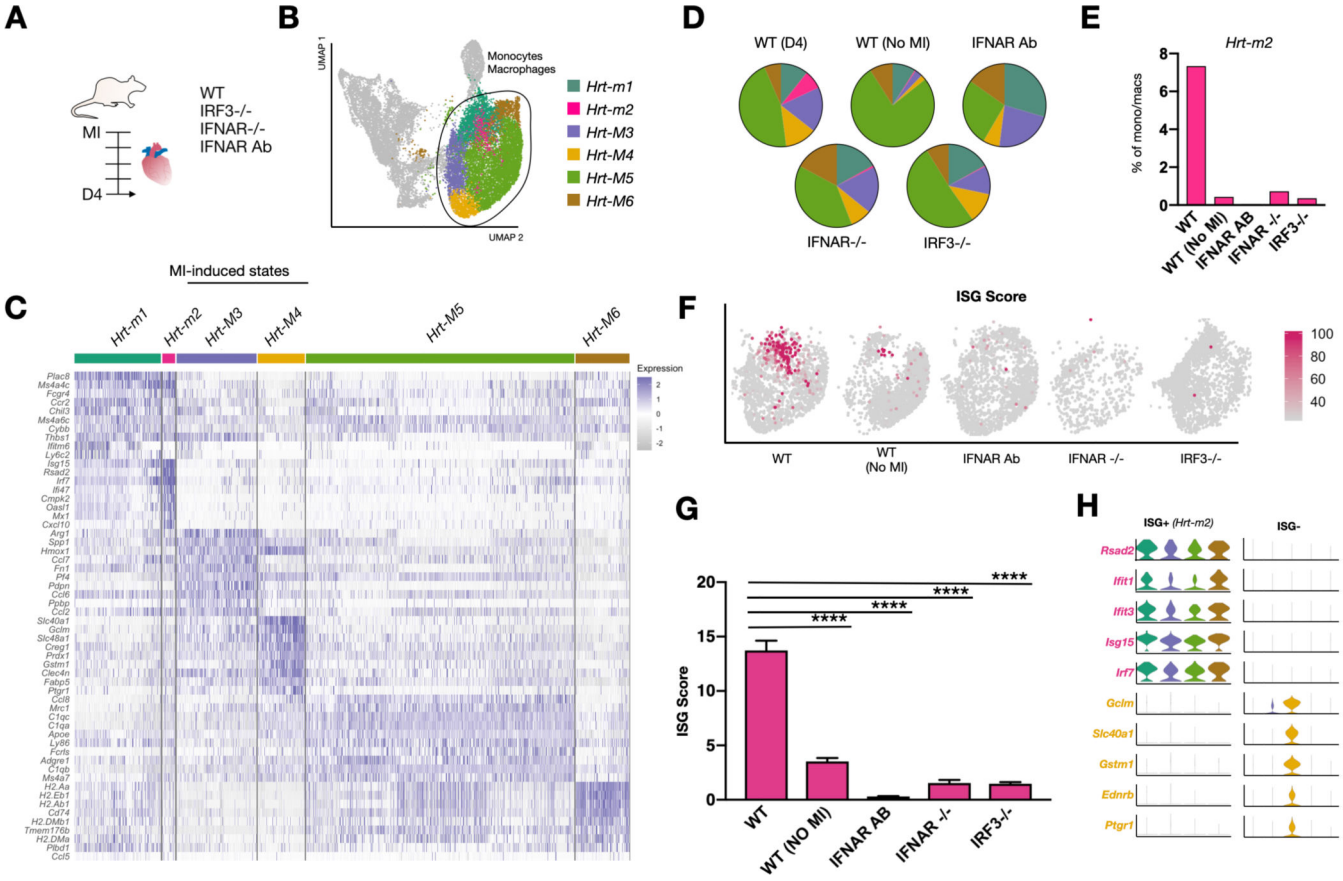

Figure 3. Intracardiac monocytes and macrophages are separable into mirrored ISG$^+$ and ISG$^-$ subsets and one non-mirrored subset within the infarcted mouse heart.

(**A**) Healthy (N=1) and infarcted hearts from WT (N=2), *Irf3*$^{-/-}$ (N=1), *Ifnar*$^{-/-}$ (N=1), and Ifnar antibody treated (N=1) mice were enzymatically digested, FACS sorted (singlets, DAPI$^-$Ter119$^-$) and barcoded for single cell RNA sequencing. (n = 20,206 total cells). Infarcts were harvested on D4-post MI. (**B**) UMAP of integrated dataset with monocytes and macrophages shown in color. (**C**) Heatmap of monocyte and macrophage subpopulations with MI-induced states noted above. (**D**) Pie charts showing distribution of subpopulations in WT, anti-Ifnar antibody treated, *Ifnar*$^{-/-}$ and *Irf3*$^{-/-}$ mice. (**E**) Percentage of Hrt-m2 (ISG$^+$) monocytes and macrophages. (**F,G**) ISG score (per cell) of monocytes and macrophages shown by UMAP (**F**) and bar plots (**G**). Data are shown as mean +/− S.E.M. (**H**) Violin plots of subclustered ISG$^+$ and ISG$^-$ cells with ISGs and Hrt-M5 marker genes. **** P< .0001, Mann-Whitney test.

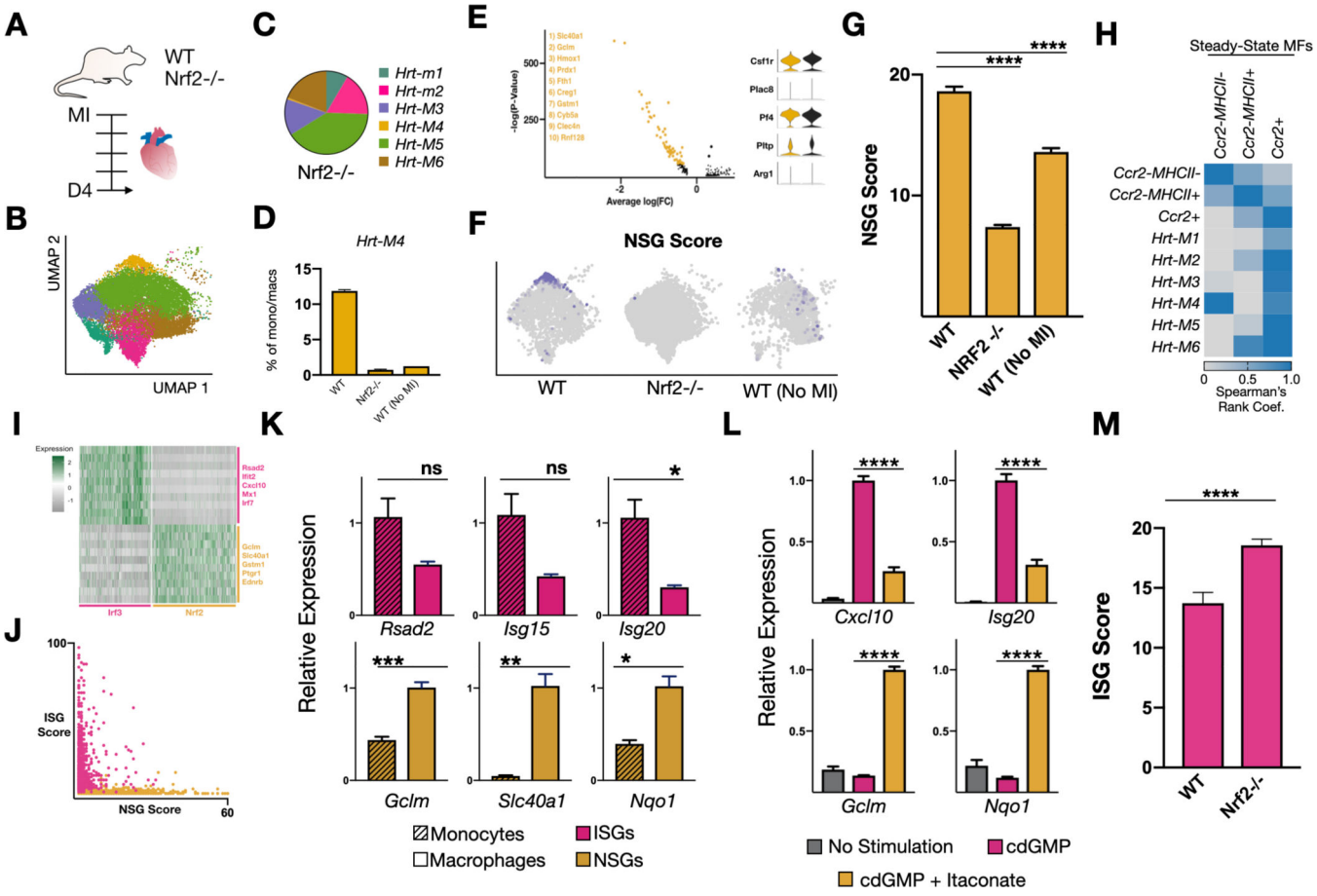

Figure 4. Nrf2-activation in non-mirrored (ISG-) steady-state macrophages limits ISG expression in the infarcted heart.

(**A**) Healthy (N=1) and infarcted hearts from WT (N=2) and *Nrf2*$^{-/-}$ (N=2) mice were enzymatically digested, FACS sorted (singlets, DAPI^{-}Ter119^{-}) and barcoded for single cell RNA sequencing (n = 25,957 total cells). Infarcts were harvested on D4-post MI. (**B**) UMAP of integrated dataset showing monocytes and macrophages (full UMAP shown in fig. S8). (**C**) Pie chart showing distribution of monocyte and macrophage subpopulation in *Nrf2*$^{-/-}$ mice. (**D**) Percentage of Hrt-M4 monocytes and macrophages. (**E**) Down-regulated genes in *Nrf2*$^{-/-}$ compared to WT macrophages. (**F,G**) Nrf2-stimulated gene (NSG) score (see methods) in WT and *Nrf2*$^{-/-}$ monocytes and macrophages. (**H**) Pearson's rank correlation coefficients comparing steady-state to post-MI mononuclear subsets. (**I**) Heatmap illustrating dichotomous expression of ISGs and NSGs in wild type mice on day 4 after MI. (**J**) Scatterplot of ISG-score and NSG-score for WT mono-mac single cells. (**K**) qPCR of ISGs (*Rsad2, Isg15, Isg20*) and NSGs (*Gclm, Slc40a1,Nqo1*) in sorted infarct monocytes (Cd11b^{+}Ly6C^{+}F4/80^{-}) and macrophages (Cd11b^{+}Ly6C^{-}F4/80^{+}). (**L**) qPCR of ISGs (*Cxcl10, Isg20*), and NSGs (*Gclm, Nqo1*) from bone marrow derived macrophages treated with cyclic-di-GMP and itaconate. (**M**) ISG scores of monocytes and macrophages from WT and *Nrf2*$^{-/-}$ mice D4 after MI. Data are shown as mean +/− S.E.M. * P< .05, ** P< .01, *** P< .001, **** P< .0001, Mann-Whitney test (**G,M**), Student's t-test (**K,L**).

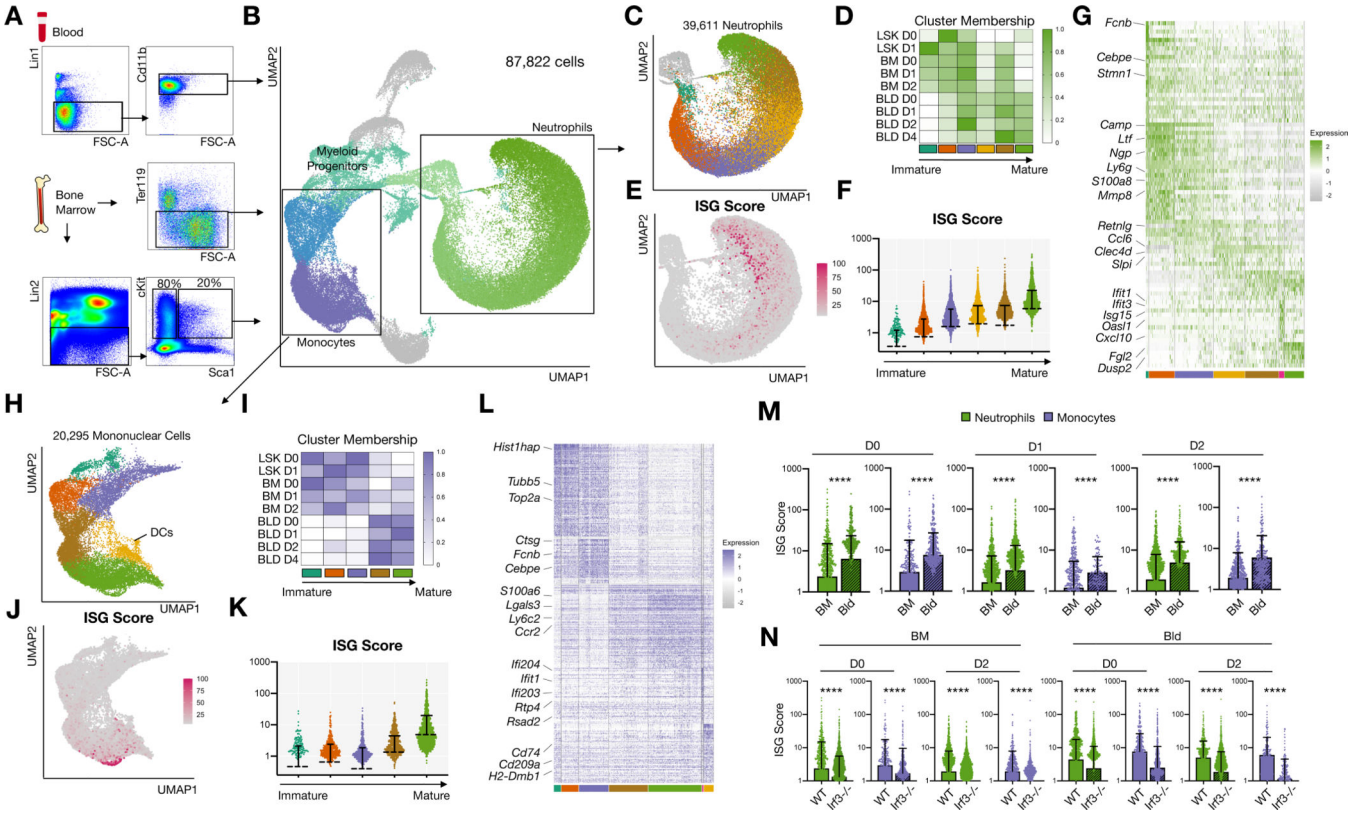

Figure 5. ISGs are expressed in myeloid cells of the murine bone marrow and blood, prior to reaching the infarcted heart.

(**A**) Bone marrow and blood leukocytes from non- and post-infarcted WT (D0, D1, D2, D4) and *Irf3*$^{-/-}$ (D0, D2) mice were FACS sorted for single cell barcoding (10X Genomics, N = 1). Lin^{-}Sca1$^{+/-}$c-Kit^{+} progenitor cells from WT (pre- and D1 post-infarct) mice were also sorted for single cell barcoding (N = 1). (**B**) Integrated UMAP plot of 87,822 cells color coded by major lineage type as indicated in plot. (**C,H**) UMAP plots of clustered (**C**) neutrophils (39,611 cells) and (**H**) monocytes (20,295 cells). (**D,I**) Cluster membership by sample (WT only, normalized by column) for (**D**) neutrophils and (**I**) monocytes. (**E,J**) Feature plots of ISG scores of (**E**) neutrophils and (**J**) monocytes. (**F,K**) Violin plots of ISG scores by cluster of (**F**) neutrophil and (**K**) monocyte populations. (**G, L**) Heatmaps showing select differential expressed genes of (**G**) neutrophil and (**L**) monocyte subsets. (**M**) ISG scores from bone marrow and blood leukocytes on D0, D1, D2 after MI. (**N**) ISG scores of bone marrow and blood leukocytes from WT and *Irf3*$^{-/-}$ mice on D0 and D2 post-MI. Data are shown as mean +/− S.D. with individual points (cells). **** P< .0001, Kolmogorov-Smirnov test.

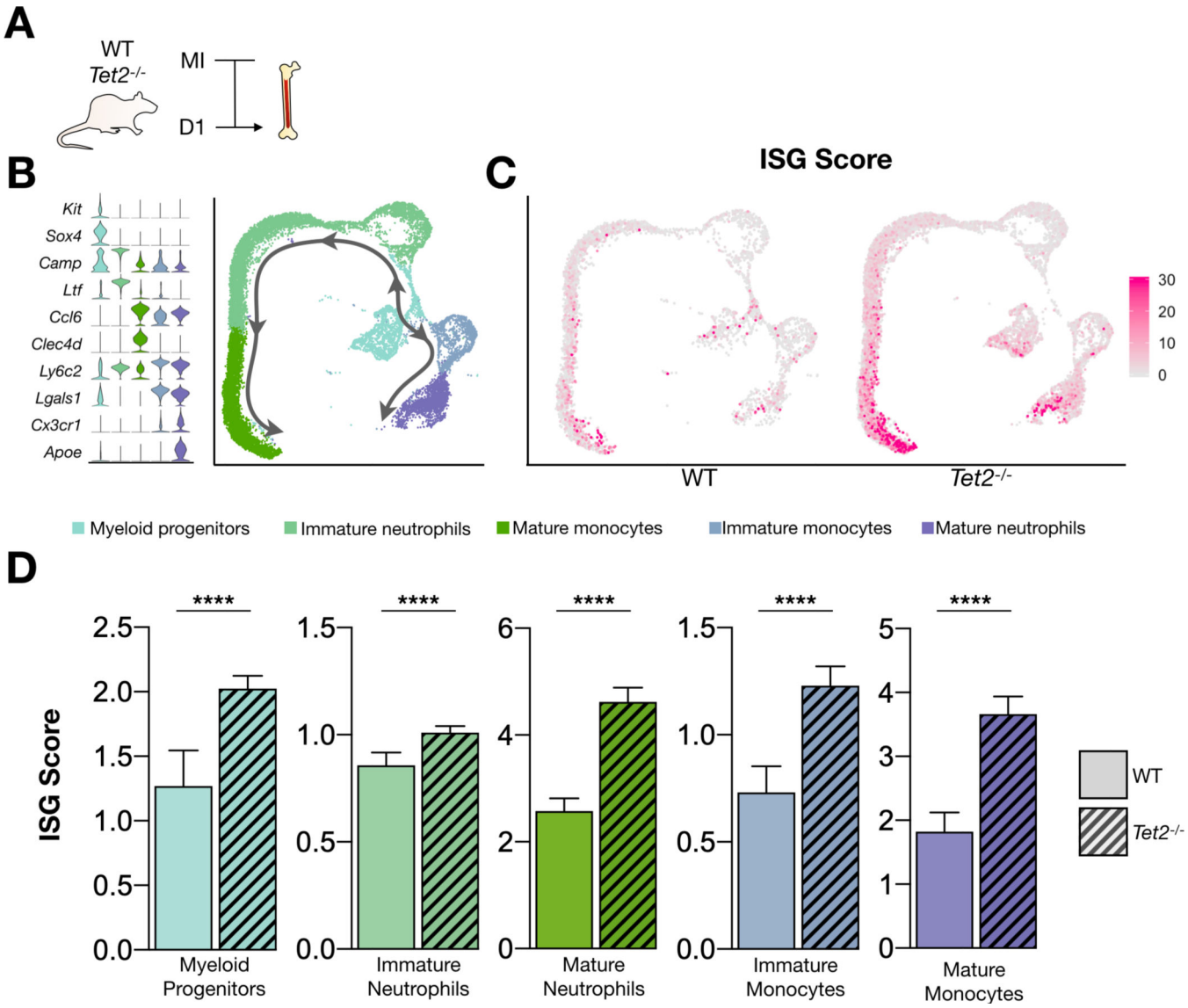

Figure 6. Tet2-deficient mice exhibit potent and spontaneous ISG induction in bone marrow myeloid progenitors and their progeny after MI.

(**A**) Schematic of experimental workflow. (**B-D**) Single-cell RNA-seq data of bone marrow myeloid cells isolated on post-MI day 1 from WT control mouse (N = 1 mouse, 4,184 cells) and *Tet2*$^{-/-}$ mouse (N = 1 mouse, 11,965 cells). (**B**) Integrated UMAP plot of all CD11b^{+} bone marrow myeloid cells enriched for Lin^{-}Sca1^{+}c-Kit^{+} cells. Violin plots depict expression of top marker genes used to annotate major cell-type identities. Arrows indicate inferred maturation trajectory along monocyte and neutrophil lineages. (**C**) Feature plot of ISG score in WT control and *Tet2*$^{-/-}$ mice after myocardial infarction. (**D**) ISG scores of bone marrow myeloid cells (split by cell type) from WT control and *Tet2*$^{-/-}$ mouse after MI. Data are displayed as mean ± SEM. **** p<0.0001, Mann-Whitney test.

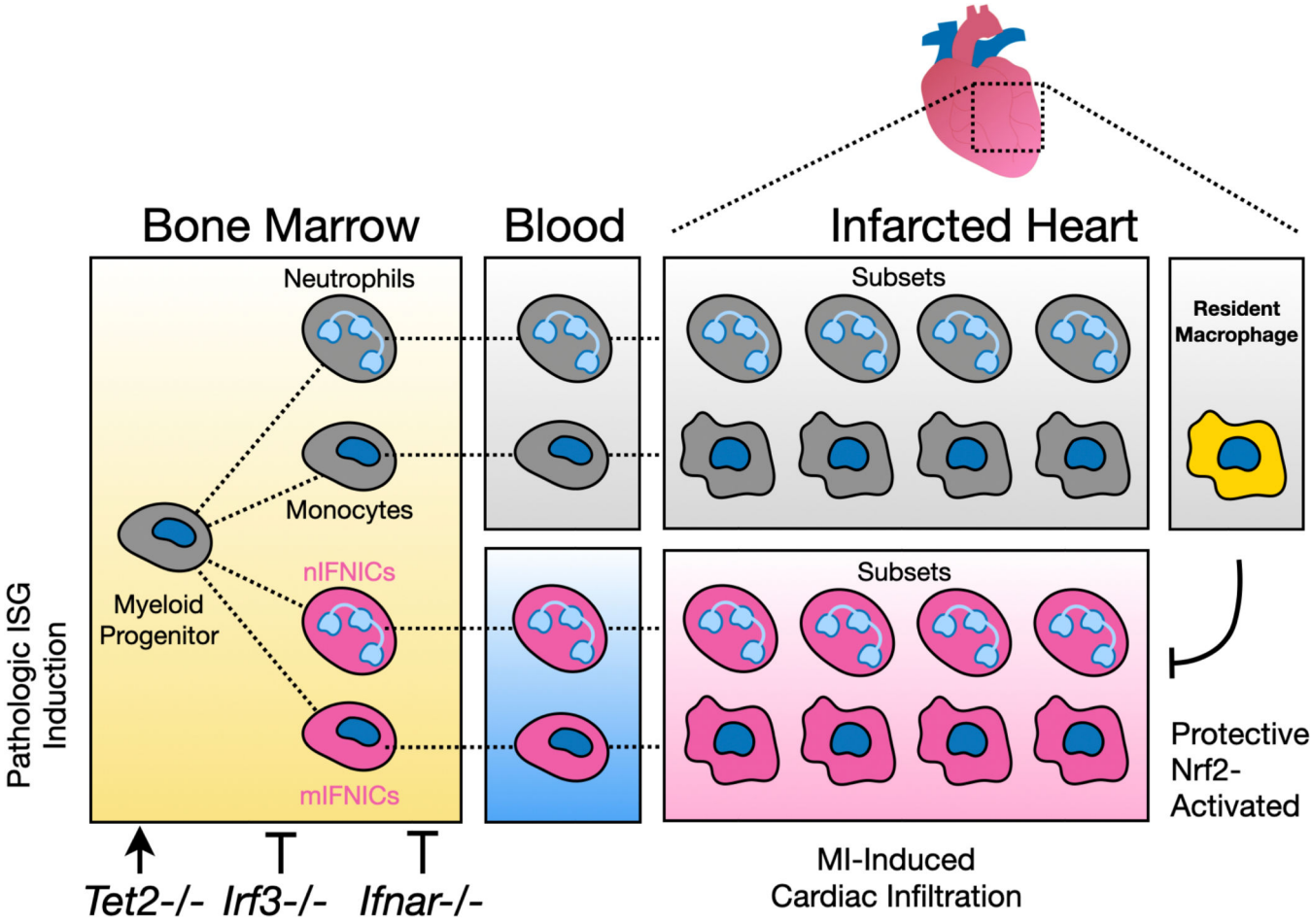

Figure 7. Myocardial infarction induces a type I interferon response in myeloid cells.

A subset of pre-neutrophils and pre-monocytes are interferon-stimulated (pink) during hematopoiesis resulting in the concerted expression of a multitude of ISGs dependent on Ifnar and Irf3. ISG expression increases with myeloid maturation and is restrained by Tet2. After myocardial infarction, ISG^{+} myeloid cells infiltrate the infarcted myocardium and specialize into several time-dependent transcriptional programs with a differentiation potential equivalent to their ISG^{-} counterparts (gray) with the exception of Nrf2 activation. In response to myocardial ischemia, a Nrf2-dependent program in cardiac macrophages negatively regulates ISG expression.